ЖЭТФ, 2005, том 127, вып. 4, стр. 752–779

EXPERIMENTAL INVESTIGATION OF MUON-CATALYZED dt FUSION IN WIDE RANGES OF D/T MIXTURE CONDITIONS

V. R. Bom[a], A. M. Demin[b], D. L. Demin[c], C. W. E. van Eijk[a], M. P. Faifman[d], V. V. Filchenkov[c], A. N. Golubkov[b], N. N. Grafov*[c], S. K. Grishechkin[b], K. I. Gritsaj[c], V. G. Klevtsov[b], A. D. Konin[c], A. V. Kuryakin[b], S. V. Medved'[c], R. K. Musyaev[b], V. V. Perevozchikov[b], A. I. Rudenko[c], S. M. Sadetsky[e], Yu. I. Vinogradov[b], A. A. Yukhimchuk[b], S. A. Yukhimchuk[c], V. G. Zinov[c], S. V. Zlatoustovskii[b]

[a] *Delft University of Technology*
2629 JB Delft, the Netherlands

[b] *Russian Federal Nuclear Center, All-Russian Research Institute of Experimental Physics*
607200, Sarov, Nizhny Novgorod Region, Russia

[c] *Joint Institute for Nuclear Research, Dzhelepov Laboratory of Nuclear Problems*
141980, Dubna, Moscow Region, Russia

[d] *Russian Research Center «Kurchatov Institute»*
123182, Moscow, Russia

[e] *St. Petersburg Nuclear Physics Institute*
188350, Gatchina, Leningrad Region, Russia

Submitted 6 September 2004

A vast program of the experimental investigation of muon-catalyzed dt fusion was performed on the Joint Institute for Nuclear Research phasotron. Parameters of the dt cycle were obtained in a wide range of the D/T mixture conditions: temperatures of 20–800 K, densities of 0.2–1.2 of the liquid hydrogen density (LHD), and tritium concentrations of 15–86 %. In this paper, the results obtained are summarized.

PACS: 36.10.-k, 36.10.Dr

1. INTRODUCTION

Investigation of the muon-catalyzed fusion (MCF) process is a unique independent direction in the modern physics relevant for molecular, atomic, and nuclear physics [1–6] and for astrophysics [7]. Study of the nuclear fusion reactions from the bound states of a muonic molecule is of great importance for determination of properties of the lightest nuclei, including various exotic nuclear systems. In addition, the high neutron yield of MCF can be effectively used for solving different practical problems such as the construction of an intense 14-MeV neutron source [8] and a nuclear fuel breeder [9].

That is why the process of MCF in hydrogen isotope mixtures has been under active study in many laboratories worldwide during the last several decades. During this period, many experimental results were obtained in investigating the muon-induced processes in different mixtures of hydrogen, deuterium, and tritium as well as in pure isotopes; most of these experimental results are in good agreement with theory. The most impressive achievement is the precise agreement between experiment and theory in the temperature dependence of the $dd\mu$-molecule formation rate in gaseous deuterium [4, 10, 11]. This allowed the binding energy of the loosely bound state of $dd\mu$ to be determined with a very high accuracy, $\epsilon_{11}^{exp} = -1962.56^{+32}_{-47}$ meV [10], which should be compared with the theoretical value

*E-mail: grafov@nu.jinr.ru

$\epsilon_{11}^{theor} = -1964.83$ meV [4].

In comparison with pure deuterium, the MCF process in a D/T mixture manifests much richer physical phenomena (the muon transfer $d \to t$ from the ground and excited states of the $d\mu$-atom, epithermal and many-body effects in the $dt\mu$-molecule formation). Theory predicts a significant increase of the $dt\mu$-molecule formation rate on the D_2 and DT molecule with the rise of temperature and density of the mixture [12, 13]. Therefore, the complete theoretical analysis requires measuring temperature and density dependences of the $d + t$ cycle parameters in as large ranges as possible. Finally, the results of the experimental and theoretic study of MCF processes in a double D/T mixture will be rather helpful for investigation and explanation of the most difficult case of the triple H/D/T mixture.

Previously, the truly systematic experimental study of the MCF process was performed at PSI only for a low-density ($\varphi \approx 0.1$ LHD, with the liquid hydrogen nuclei density LHD $= 4.25 \cdot 10^{22}$ cm^{-3}), low-temperature ($T < 300$ K) gaseous D/T mixture [14]. The same group, as well as the RIKEN-RAL team, made measurements with liquid and solid D/T mixtures [15, 16]. The only group that investigated MCF in the high-density ($\varphi \approx 1$ LHD), high-temperature ($T \leq 600$ K) mixtures was the LAMPF team [17, 18]. But its measurements had a «prompt» character and caused many questions on the analysis. We therefore decided to conduct a full set of measurements in a wide region of the experimental conditions spanning the density range $\varphi = 0.2$–1.2 LHD and the temperature range $T = 20$–800 K.

The Dzhelepov Laboratory of Nuclear Problems made a prominent contribution to the MCF experimental study. The Dubna group discovered the phenomenon of the $dd\mu$-molecule resonance formation [19] and later directly confirmed its existence by measurements of the temperature dependence of the $dd\mu$-molecule formation rate [20]. This group was the first to experimentally investigate [21] the muon-catalyzed fusion

$$dt\mu \longrightarrow {}^4\mathrm{He}(3.5\ \mathrm{MeV}) + n(14.1\ \mathrm{MeV}) + \mu$$

and to confirm the theoretical predictions [22] of the high intensity of this process which induced the activity in the MCF study worldwide.

Since 1997, our collaboration has been carrying out a large program of investigation of MCF processes in D/T at the JINR Phasotron. The distinctive characteristic of our study is the use of novel methods both in the measurements and in the experimental data analysis, which allows us to obtain accurate and reliable data not worse than those obtained at meson facilities. The experimental method that we used made it possible to measure the MCF cycle parameters in the D/T mixture under a wide variety of mixture conditions [23].

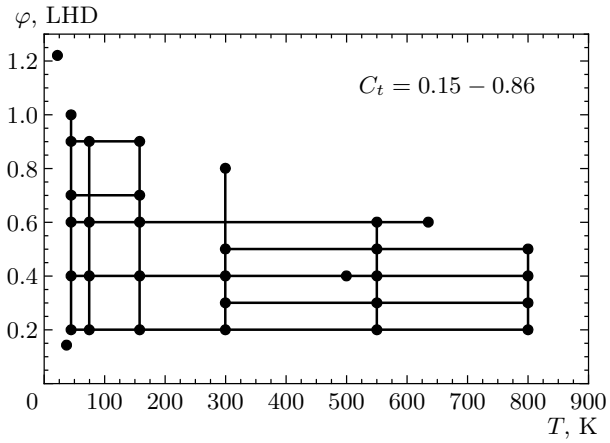

Fig. 1. The experimental conditions (density and temperature) for the MCF process study in the D/T mixtures

This paper is a report on the most comprehensive measurements of the MCF parameters in the D/T mixture. The preliminary data were published in [23–26]. Figure 1 shows the condition ranges of the experiments conducted up to now. The accumulated data and the MCF cycle parameters cover wide ranges of D/T mixture conditions:

1) temperatures of 20–800 K;
2) tritium concentrations of 15–86 %;
3) densities of 0.2–1.2 LHD.

2. GENERAL DESCRIPTION OF THE PROCESS

The simplified scheme of MCF kinetics in a double D/T mixture is shown in Fig. 2. Muons stopped in the mixture form $d\mu$- and $t\mu$-atoms in their ground states with the respective probabilities

$$w_{d\mu} = C_d q_{1S}$$

and

$$w_{t\mu} = C_t + C_d(1 - q_{1S}) = 1 - C_d q_{1S},$$

where C_d and C_t are relative hydrogen isotope concentrations and q_{1S} is the fraction of $d\mu$-atoms in the ground state after muon cascade processes, with the

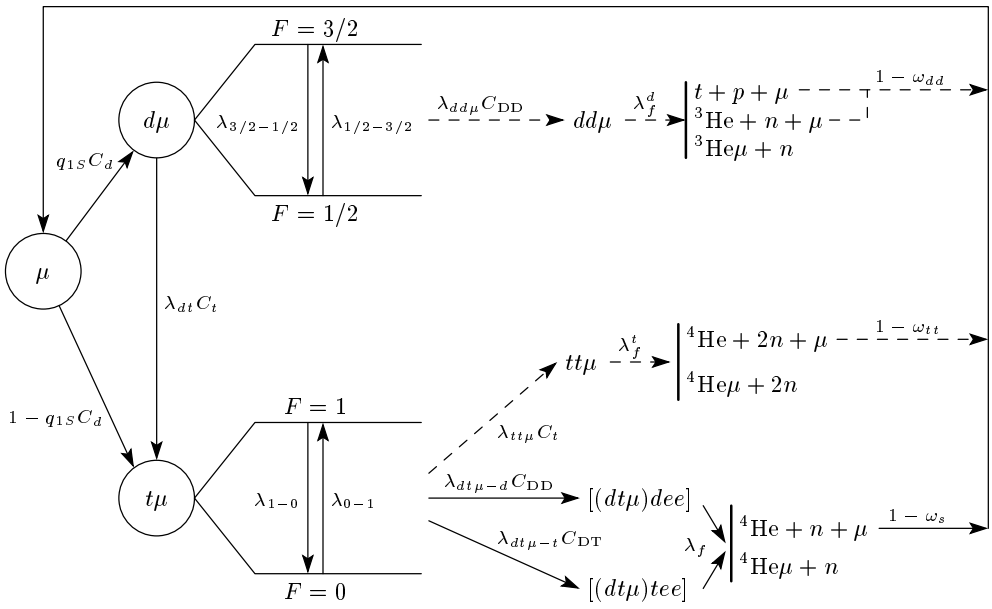

Fig. 2. Scheme of the MCF kinetics in the double D/T mixture

muon transfer $(d\mu)_n \to (t\mu)_n$ from $d\mu$ to $t\mu$ during the de-excitation cascade taken into account [27–29]:

$$q_{1S} = \frac{\lambda_{dex}}{\lambda_{dex} + \lambda_{tr}}. \tag{1}$$

Here, λ_{dex} and λ_{tr} are the rates of de-excitation and muon transfer averaged over the $d\mu$-atom excited states. One should expect strong dependence of q_{1S} on C_t and φ [30, 31].

The «standard» cascade model, in which the initial μ-atom energies are distributed around $E_0 = 1$–2 eV, is apparently valid only at very low densities $\varphi \le 10^{-3}$ LHD. Now it is known that during the cascade, muonic atoms can be both thermalized and accelerated, obtaining the energy as high as tens of eV (see, e.g., [32–34]). But until now, the problem of determining the initial energy distribution of muonic atoms after the cascade has not been solved definitely.

Being in the $d\mu$-atom ground state, the muon can be transferred to tritium in the collisional process

$$d\mu + t \longrightarrow t\mu + d \tag{2}$$

with the rate $\lambda_{dt} = 2.8 \cdot 10^8\ {\rm s}^{-1} \cdot \varphi$ [18, 21, 35, 36]. In transfer process (2), the $t\mu$-atom acquires the energy 19 eV. The atoms $t\mu$ are formed in two hyperfine states with the total spin $F = 1$ (weight 0.75) and $F = 0$ (weight 0.25) and can take part in the spin-flip processes

$$(t\mu)_{F=1} + t \longleftrightarrow (t\mu)_{F=0} + t. \tag{3}$$

Muonic atoms $t\mu$ can form $dt\mu$- and $tt\mu$-molecules and $d\mu$-atoms can form $dd\mu$-molecules. In these μ-molecules, fusion reactions occur, in which the muon can be released and stimulate the next MCF cycle or stick to helium produced in the reactions. The notation for the rates of muonic formation and fusion reactions as well as for the sticking probabilities is introduced in Fig. 2. Being bound in a μ-atom or a μ-molecule or being free, the muon disappears with the rate $\lambda_0 = 4.55 \cdot 10^5\ {\rm s}^{-1}$.

The specific feature of the $dd\mu$- and $dt\mu$-molecule formation processes is their resonance character, that is, the muonic molecular formation rates $\lambda_{dd\mu}$ and $\lambda_{dt\mu}$ turn out to depend on the μ-atom kinetic energy [3]. The MCF $d + d$ cycle has been studied very well. The measured temperature dependence $\lambda_{dd\mu}(T)$ is in excellent agreement with theory [13].

Quite a different situation occurs for the MCF $d + t$ cycle. In fact, this process has been studied in detail in the parameter region (low temperatures) where the «standard» theory predicts its relatively low intensity. It follows from experiment that just in this region the MCF process is very effective. Modern theory explains this only qualitatively.

It follows from the original Vesman consideration [37] that the resonance $dt\mu$-molecule formation occurs in the interaction of the $t\mu$-atom with D_2, DT or HD molecules according to the scheme [22]

$$t\mu + (\mathrm{DX})_{K_i} \longrightarrow [(dt\mu), x, 2e]_{\nu, K_f} \qquad \mathrm{X} = \mathrm{H,D,T} \quad x = p, d, t, \tag{4}$$

where the energy released under $dt\mu$ formation together with the $t\mu$-atom kinetic energy $E_{t\mu}$ is transferred to excite the vibration–rotational state of the molecular complex $[(dt\mu), x, 2e]$. Here, K_i and K_f are the respective rotational quantum numbers of the «initial» molecule DX and the «final» complex. The set of the resonance $t\mu$-atom energies

$$E^r_{t\mu} = \Delta E_{\nu,K}$$

corresponds to different transitions $\nu = 3, 4, 5$; $K_i \to K_f$. Indeed, the spin states of the $t\mu$-atom and the $dt\mu$-molecule should be taken into account for determination of $E^r_{t\mu}$. In addition, the position and intensity of the resonances depend on the type of the molecule (D_2, DT, and HD) and the temperature of the mixture influencing the population of the rotational states of these molecules.

Being formed, the complex $[(dt\mu), x, 2e]$ either undergoes the back decay

$$[(dt\mu), x, 2e] \to t\mu + \mathrm{DX}$$

or the fusion reactions

$$dt\mu \longrightarrow {}^4\mathrm{He} + n + \mu, \tag{5}$$

$$dt\mu \longrightarrow {}^4\mathrm{He}\mu + n \tag{6}$$

take place in it (with the high rate $\lambda_f \approx 10^{12}$ s^{-1} [38]). The muon-to-helium sticking probability is $\omega_s \approx 0.5$ %.

The resonance dependences $\lambda_{dt\mu-p,d,t}(E_{t\mu})$ for the $t\mu$-atom of spin $F = 0$ are shown in Fig. 3; the calculations presented there are based on the evaluation scheme developed in [13]. The following remarkable features are evident from this figure.

1. Resonance formation of the $dt\mu$-molecule on HD molecules is most intensive.

2. The resonance positions correspond to relatively high $t\mu$-atom energies, that is, to high temperatures ($T \sim 10^3$ K) for the thermalyzed muonic atoms.

3. The positions of the resonances of each type correspond to various vibration levels of the complex $\nu = 3, 4, 5$. The nearest resonance for $\lambda^0_{dt\mu-d}$ is placed at $E_{t\mu} \approx 0.5$ eV. This means that the nearest «sub-threshold» resonance (corresponding to $\nu = 2$) is close to zero at the negative $t\mu$-atom energy $E_{t\mu} \approx -(10\text{–}12)$ meV. Negative energy implies that for the most intensive dipole transitions $|K_f - K_i| = 1$, an energy excess arises that cannot be transferred in two-particle reaction (4).

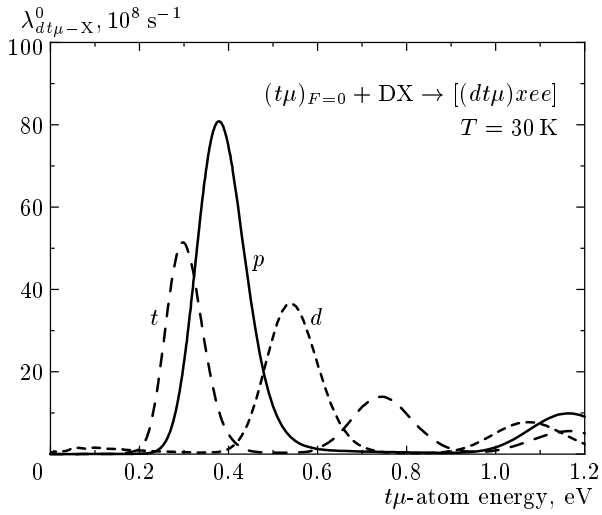

Fig. 3. The $dt\mu$-molecule formation rates on D_2, DT, and HD molecules for the $t\mu$-atom spin $F = 0$ as a function of $E_{t\mu}$ for $T = 30$ K (calculations based on [13])

For the highest multiple transitions ($\nu = 2$; $K_i = 0, 1 \to K_f = 2, 3, 4$), process (4) becomes possible but its intensity is two orders of magnitude lower than that of the main transitions. But in contradiction with the «standard» theory, experiment manifests high MCF intensity in the low temperature D/T mixture and reveals a nontrivial density dependence of its cycling rate. We note that the highest value of the cycling rate $\Lambda_c = 185 \pm 13\ \mu\mathrm{s}^{-1}$ was measured at PSI [15] in a solid D/T mixture.

This can be qualitatively explained in the modern theory [39], according to which the influence of the sub-threshold resonance turns out to be much stronger due to the mechanism of triple collisions. According to the theory, the resonance $dt\mu$ formation at low temperatures occurs at sub-threshold resonance in the triple collision process

$$t\mu + \mathrm{D}_2 + \mathrm{M} \longrightarrow [(dt\mu), d, 2e] + \mathrm{M}', \qquad \mathrm{M} = \mathrm{D}_2, \mathrm{DT}, \mathrm{T}_2\,. \tag{7}$$

The «additional» second molecule M plays the role of a spectator that carries away the energy excess away. Because (7) is a three-particle process, it must depend on the density of molecules M.

Qualitatively the scheme in (7) explains both the high values of $\lambda_{dt\mu-d}$ and its density dependence observed in experiment. However, in spite of many efforts undertaken to calculate its intensity (see, e.g., [40, 41]), the quantitative explanation is not yet obtained.

With the temperature increase, the resonance pic-

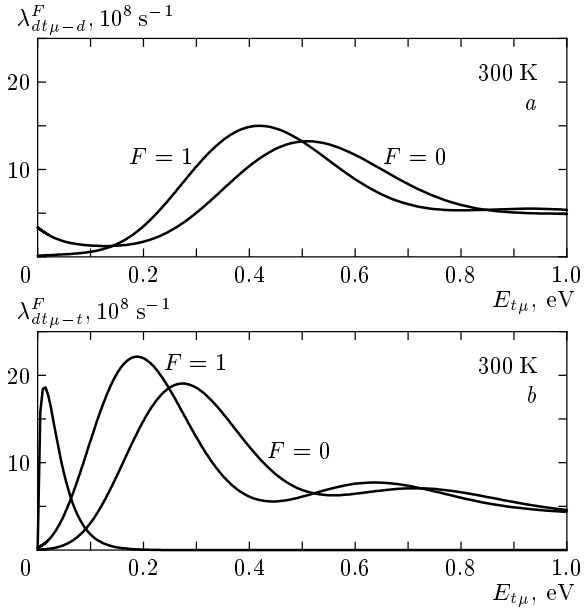

Fig. 4. The dependence of $\lambda_{dt\mu-d}$ (a) and $\lambda_{dt\mu-t}$ (b) on the $t\mu$-atom energy for $T = 300$ K. The Maxwell distribution is shown in the bottom picture

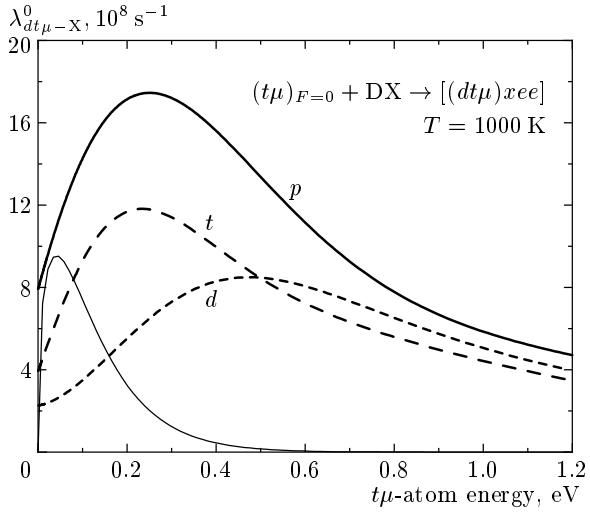

Fig. 5. The $dt\mu$-molecule formation rates on D_2, DT, and HD molecules for the $t\mu$-atom spin $F = 0$ as a function of $E_{t\mu}$ for $T = 1000$ K (calculations based on [13]) and the Maxwell distribution

tures are modified due to the change of the population of the DX molecule rotational states and the thermal motion of the molecule. The calculated rates $\lambda_{dt\mu-d}$ and $\lambda_{dt\mu-t}$ as functions of $E_{t\mu}$ for $T = 300$ K are presented in Fig. 4. The Maxwell distribution for the thermalyzed $t\mu$-atoms is shown in one of them ($\lambda_{dt\mu-t}$). As is seen, this distribution only slightly overlaps the nearest resonance.

The resonances for $\lambda_{dt\mu}$ at $T = 1000$ K are presented in Fig. 5. In this case, the Maxwell distribution considerably overlaps the most intensive resonances for the $dt\mu$ formation on D_2, DT, and HD molecules. Unfortunately, this high temperature is not yet achieved in experiment. The temperature $T = 800$ K is the highest at which the measurements were made (in Dubna).

As we have mentioned, a substantial part of $t\mu$ has the initial (after cascade) energy $E_{t\mu} > 1$ eV. In elastic collisions $t\mu+t$, $t\mu+d$, these atoms are quickly thermalyzed. The thermalization time is approximately equal to ns for the 1 LHD of a mixture. Accordingly, the time distribution of the fusion reaction products (neutrons) should have two components: a quick «spike» corresponding to the first pass through the resonances and a much slower «steady-state» component.

Due to shortness of the epithermal spike and ambiguity in the initial energy of the $t\mu$-atom, it is difficult to interpret this effect. That is why the main efforts of different experimental groups were concentrated on the steady-state study, for which the $t\mu$-atom energy spectrum is a Maxwell distribution.

For convenience, the comparison of the measurements with the theoretical calculations is performed for the so-called «effective» $dt\mu$-molecule formation rate as a function of temperature. It is obtained by integrating over all possible initial states, averaging over all final states, and convolving with the Maxwell spectrum $W(E_{t\mu}, T)$. Such calculations for the D/T mixture were made in [13].

For the steady state, the time distribution of fusion neutrons has the form

$$\frac{dN_n}{dt} = N_\mu \epsilon_n \Lambda_c \exp(-\lambda_n t), \quad \lambda_n = \lambda_0 + w\Lambda_c, \qquad (8)$$

where $\Lambda_c = \lambda_c \varphi$, ϵ_n is the neutron detection efficiency, N_μ is the number of muons stopped in the D/T mixture, and ω is the muon loss in the cycle, which is the probability of muon sticking to helium in fusion reactions, mainly in $d+t$ (ω_s), and also, with lower weight, in the accompanying reactions $d+d$ and $t+t$. The cycling rate Λ_c means the inverse of the average time between the closest cycles. It involves mainly the time of $d\mu$ to $t\mu$ transfer (2), $t\mu$-atom spin-flip process (3), and $dt\mu$-molecule formation (4). The neutron yield Y_n is limited by ω and λ_0:

$$Y_n^{-1} = \omega + \frac{\lambda_0}{\Lambda_c}. \qquad (9)$$

The expression for λ_c, corresponding to the kinetic scheme of Fig. 2, is

$$\frac{1}{\lambda_c} \approx \frac{q_{1s}C_d}{\lambda_{dt}C_t} + \frac{0.75}{\lambda_{1-0}C_t} + \\ + \frac{1}{\lambda_{dt\,\mu-d}C_{\mathrm{DD}} + \lambda_{dt\mu-t}C_{\mathrm{DT}}}. \quad (10)$$

To extract the values $\lambda_{dt\mu-d}$ and $\lambda_{dt\mu-t}$, one should use formula (10) to analyze the experimental values of λ_c measured at different tritium concentrations changing the relative population of D_2 and DT molecules.

The expression for ω is

$$\omega \approx \omega_s + \frac{\lambda_{tt\mu}C_t\omega_{tt}}{\lambda_{dt\mu-d}C_{\mathrm{DD}} + \lambda_{dt\mu-t}C_{\mathrm{DT}} + \lambda_{tt\mu}C_t} + \\ + \frac{q_{1s}C_d\dfrac{2}{3}\lambda_{dd\mu}^{3/2}C_{\mathrm{DD}}\omega_{dd}r}{\lambda_{dt}C_t + \lambda_{dd\mu}^{3/2}C_{\mathrm{DD}} + \lambda_{3/2-1/2}C_d} + \frac{\lambda_Z C_Z}{\lambda_c}, \quad (11)$$

where λ_Z is the rate of muon transfer to possible admixtures with $Z > 1$, having concentration C_Z, $\lambda_{dd\mu}^{3/2}$ is the rate of $dd\mu$-molecule formation from the $d\mu$-atom state with spin $F = 3/2$, and r is the branching ratio of the dd fusion channels ($^3\mathrm{He} + n$) and ($t + p$); the other variables are defined in Fig. 2. It follows from Eq. 11 that the minimum value of ω is achieved at highest λ_c (large λ_{dt} and $\lambda_{dt\mu-d,t}$), where ω is close to its natural limit $\omega_s \approx 0.5\,\%$.

We note that in expressions (10) and (11) and in what follows, the cycling rate and all collisional rates are normalized to the nuclear density φ of the D/T mixture.

3. EXPERIMENTAL METHOD

All experimental runs were made at the installation «Triton» mounted on the muon channel [42] of the JINR phasotron. The experimental setup is schematically shown in Fig. 6. The novel experimental method in [23] was used. Based on measurements of the total charge produced by the fusion neutrons in a detector, it allowed us to avoid the distortions in the neutron time spectra caused by the pile-up and thus to use a high-efficiency detection system.

Incoming muons are detected by scintillation counters *1*, *2*, *3*, a proportional wire counter *4* and stopped in the target. Neutrons from the $d-t$ reaction are detected by two full-absorption neutron detectors *ND1* and *ND2*. Electrons from the decay of muons stopped in the target are registered by the proportional wire counter *5* and scintillation detectors *1-e* and *2-e*.

3.1. The specific features of the method

The following important features characterize the method used.

1. Unique targets and tritium handling system were used, which allowed measurements in a wide range of the D/T mixture densities and temperatures.

2. A high-efficiency neutron detection system was used in the geometry close to 4π. It provided a high counting rate and low accidental background.

3. A specially designed proportional counter was used for muon and electron detection; having a low sensitivity to neutrons, it allowed reliable electron identification.

4. Time distributions of charge were measured instead of the usually registered time spectra of the number of events. Flash ADC were used for this aim. This allowed us to avoid distortions in the neutron time spectra and thus to use a high-efficiency detection system.

5. The novel analysis methods were used, which turned out to be most effective for the high neutron multiplicity realized in the experiment. In addition to the usually measured neutron time distribution, we measured and analyzed the neutron multiplicity distribution and the spectra of the time between the μ-decay electron and the last neutron in the series. This allowed us to decrease systematic errors and to obtain reliable data.

3.2. Targets and gas handling system

A set of targets [43–45] with the working volume 10–18 cm^3 depending on the tritium content was used in the experiments. The targets allowed the following measurements:

1) with liquid D/T (the liquid tritium target (LTT) [43] of 18 cm^3, working temperature 20–40 K, pressure up to 20 bar);

2) with hot gaseous D/T (the high-pressure tritium target (HPTT) [44] of 16 cm^3, working temperature 300–800 K, pressure up to 1600 bar);

3) with cold gaseous D/T (two high-pressure tritium targets (HPTT) [45] of 8 and 16 cm^3, working temperature 40–200 K, pressure up to 2500 bar).

The special cryogenic system [43] (for the LTT and HPTT) and the cryorefrigerator (for the HPTT) were used at low temperatures ($T < 300$ K) and the system of special heaters was used at high temperatures to maintain the needed temperature regime. Cryogenic filling was used for all targets.

A special preparation system based on palladium filters [46] provided the gas of the required composition

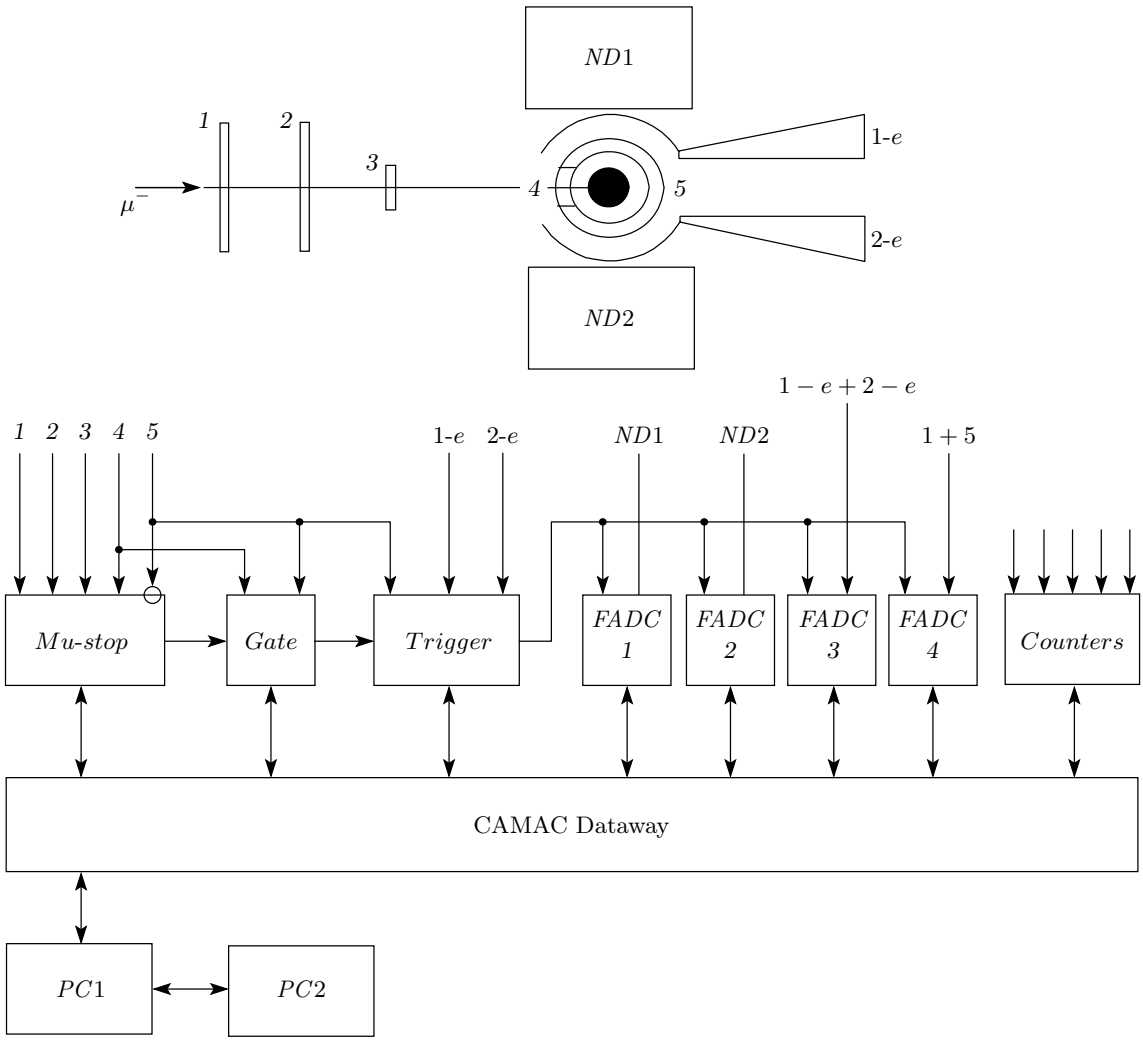

Fig. 6. Experimental layout

and purified of impurities at the level less then 10^{-7} of volume parts. The molecular composition of the mixtures was monitored with the aid of chromatography.

3.3. Detectors and electronics

The target was surrounded by a set of detectors. Scintillation counters *1–3* detected incoming muons. A cylinder-shaped proportional counter (PC, analogous to [47]) with wires grouped in two parts (*4*, *5*) served to select muon stops in the target (signal $1{\cdot}2{\cdot}3{\cdot}4{\cdot}\bar{5}$) and to detect electrons from the muon decay. Specially designed cylinder-shaped scintillation counters (*SC*) *1-e* and *2-e* were used to detect μ-decay electrons in coincidence with counter *5* (signals $5 \cdot$ *1-e* and $5 \cdot$ *2-e* were considered as a μ-decay electron). The full-absorption neutron spectrometer [48, 49] consisting of two large detectors (*ND1* and *ND2*) with the volume 12.5 l each was the basis of the detection system. It was aimed at detecting neutrons from reactions (*5*, *6*). A plastic scintillator with dimensions ($\oslash 31 \times 17$) cm was used in each detector. It was viewed by four PMs XP 2040. The direct contact of the PMs with the scintillator and teflon used as an optical reflector provided excellent spectrometric properties of the detector. Its energy resolution was

$$\sigma_{FWHM} = 0.09\left(1 + 1/\sqrt{E_e\ [\mathrm{MeV}]}\right).$$

The total solid angle covered by two detectors was $\Omega \approx 70\,\%$, which corresponded to the total neutron detection efficiency $\epsilon_n \approx 2 \cdot 15\,\%$. The time resolution of *ND* was dictated by the light collection process and electronics and was $\Delta t = 6$–7 ns.

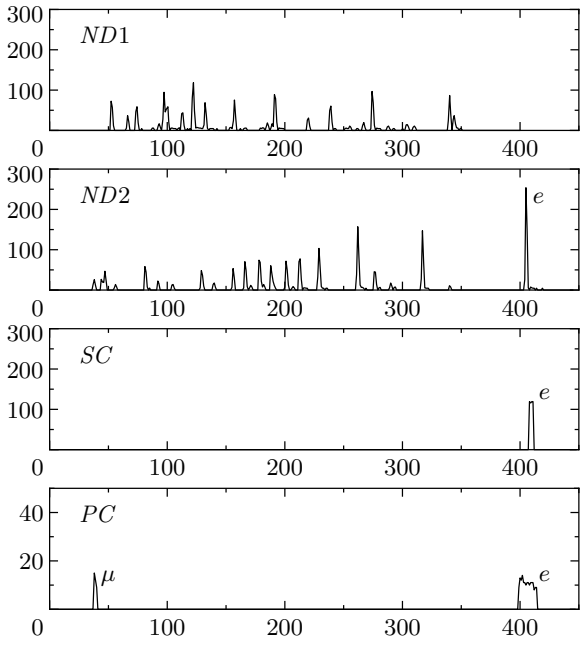

Fig. 7. Flash ADC signals for a single muon

The trigger [50] allows recording only those events for registration that were connected with an electron detection. Because the intensity of the process under study was high, these events were accompanied by neutron detection practically in each case.

The trigger requirements included the presence of the muon stop signals (*1*, *2*, *3*, *4*, $\bar{5}$) and electron signals (*5*, *1*-*e* or *5*, *2*-*e*) during the time gate 20 μs long started by the incoming muon signal (*1*, *2*). Insertion of the electron signal in the trigger makes it possible to radically suppress the background connected with the muon stops in the target walls, where muon undergoes predominately (90 %) nuclear capture without electron escape. Additional suppression of this background is achieved under the condition that only delayed electrons (later than 0.2 μs after the gate start) are permitted.

Another important advantage of this is that the direct normalization to the electron number becomes possible without the necessity to determine the number of muon stops in hydrogen. This method was first employed by us in the first experiment on the MCF $d+t$ reaction [21] and allows successful accomplishment of this fundamental work.

Pulses from the neutron spectrometer are registered by the flash ADC (8 bits $\times$2048 samples, 100 Mc/s) producing a time distribution of the *ND1*, *ND2* signal amplitude for each single muon. To provide correct time measurements, the signals of the detector for incoming muons and the electron counter are also analyzed by the flash ADC. An example of «oscillogramms» observed at the flash ADC is shown in Fig. 7. During each run, the on-line monitoring of data accumulation was conducted.

4. EXPERIMENTAL CONDITIONS

A total of 81 exposures with D/T mixtures were carried out. The conditions (density, temperature, and tritium concentration) of each run are presented in Table 1. In each exposure (duration of 6–10 hours), at least 20000 electrons from the decay of muons stopped in the target were accumulated. In practically all cases, the neutron statistics was sufficiently large. The special exposures with empty targets were carried out to measure background of electrons from muons stopped in the target walls.

4.1. Temperature and pressure control

Temperature of liquid D/T was determined by measuring the D/T vapor pressure with the tensometric gauges having the accuracy 0.5 %. Hence, the D/T temperature was determined with the accuracy 0.1 K. The temperature of gaseous D/T was measured by special thermocouples. During the experimental runs, a small temperature gradient existed in the D/T mixture, which was taken into account in the determination of temperature and its error. The accuracy of determining the temperature was 3–10 K in the 40–800 K range. Pressure was measured with the use of strain pressure gauges having the calibration error 3 %.

4.2. D/T mixture density

Nuclear density of liquid D/T was determined using the cryogenic data on deuterium and tritium [51] taking the mixture content into account. Errors in density were 2 %.

Nuclear density of gaseous D/T was determined by two ways. The first was the use of the deuterium (tritium) equation of state [52], with the gas temperature and pressure known from measurements. Some corrections for the presence of the buffer volume having room temperature was made. The second way was the density determination via the quantity of gas in the target of a known volume. Both methods gave identical results within the accuracy of 4 %. The final error of gas density was up to 3–4 %.

Table 1. Normalized cycling rates λ_c, muon loss probabilities ω and neutron yields per muon Y_n. For λ_c the uncertainties due to statistics, density ($\Delta\varphi$), charge calibration procedure (Δq) and the total uncertainty are indicated. For all parameters the total errors include the systematic uncertainty in the determination of neutron detection efficiency ($\Delta\epsilon_n = 6\,\%$)

№	Conditions		ω, %	Y_n	Error contributions, %				
	φ, LHD	C_t, %			λ_c, μs^{-1}	Stat.	$\Delta\varphi$	Δq	Total
$T = 22.0 \pm 0.7$ K (liquid)									
1	1.19	18.1(1.5)	0.77(0.07)	68.9(5.9)	61.5	0.4	2.1	3.1	7.7
2	1.20	33.4(1.0)	0.72(0.06)	96.6(7.9)	117.7	0.2	2.1	3.1	7.7
3	1.19	35.2(1.0)	0.63(0.05)	102.9(8.6)	117.9	0.3	2.1	3.1	7.7
4	1.23	63.5(2.0)	0.76(0.07)	82.5(6.9)	84.6	0.4	2.4	3.1	7.8
5	1.24	85.5(2.5)	1.40(0.11)	34.2(2.8)	20.8	0.6	2.4	3.1	7.8
$T = 38.5 \pm 2.0$ K									
6	0.143	57.0(2)	1.03(0.08)	10.1(0.8)	31.1	1.5	3.3	3.1	8.2
$T = 45 \pm 2$ K									
7	0.237	31.4(0.5)	0.77(0.06)	32.0(2.6)	80.5	1.0	3.4	3.4	8.3
8	0.449	16.7(0.5)	0.81(0.06)	39.4(3.2)	59.9	1.0	3.0	3.2	8.1
9	0.450	31.4(0.5)	0.68(0.05)	54.2(4.5)	88.7	0.9	3.3	3.4	8.3
10	0.448	50.6(0.5)	0.81(0.06)	43.8(3.6)	73.1	1.3	3.0	3.2	8.1
11	0.445	71.1(0.5)	1.46(0.11)	19.0(1.6)	30.6	1.3	2.9	3.2	8.1
12	0.689	16.3(0.5)	1.12(0.09)	46.1(3.7)	64.2	0.9	3.0	3.1	8.0
13	0.643	31.1(0.5)	0.74(0.06)	69.9(5.8)	101.2	0.7	3.3	3.4	8.2
14	0.704	52.7(0.5)	1.11(0.09)	53.4(4.2)	84.0	0.7	3.0	3.1	8.0
15	0.766	71.2(0.5)	1.89(0.15)	27.5(2.2)	34.7	1.3	3.0	3.1	8.1
16	1.022	16.3(0.5)	1.55(0.12)	45.0(3.5)	65.2	1.0	3.0	3.1	8.0
17	0.912	31.1(0.5)	0.89(0.07)	76.0(6.3)	118.5	0.8	3.2	3.4	8.2
18	1.024	52.7(0.5)	1.12(0.09)	64.2(5.0)	97.7	0.8	3.0	3.1	8.0
19	1.018	71.2(0.5)	1.83(0.14)	34.2(2.7)	40.6	1.1	3.0	3.1	8.1
$T = 75 \pm 2$ K									
20	0.234	31.4(0.5)	0.85(0.07)	29.8(2.5)	81.2	1.0	3.0	3.4	8.2
21	0.445	31.4(0.5)	0.87(0.07)	50.4(4.2)	92.1	0.9	2.9	3.4	8.1
22	0.635	31.4(0.5)	0.94(0.07)	69.9(5.8)	101.6	0.7	3.0	3.4	8.1
23	0.897	31.1(0.5)	0.91(0.07)	75.5(6.2)	119.5	0.8	3.0	3.4	8.1

In addition, we have another way to check the mixture density. If the muon beam intensity is stable, the number of muon stops in the mixture per time unit is proportional to the mixture density. In several cases, we made some corrections (about few percent) to the mixture density based on this method.

4.3. Measurements of isotope and molecular gas composition

The chromatographical method [53] was used to control the isotope and molecular composition of the mixtures. In addition, an ionization chamber was used to obtain the D/T and T_2 content. Measurements were

Continuation of Table 1

№	Conditions		ω, %	Y_n	Error contributions, %				
	φ, LHD	C_t, %			λ_c, μs^{-1}	Stat.	$\Delta\varphi$	Δq	Total
$T = 158 \pm 2$ K									
24	0.230	31.4(0.5)	0.94(0.07)	28.6(2.4)	79.3	1.1	3.0	3.4	8.2
25	0.438	16.7(0.5)	1.41(0.11)	31.0(2.5)	58.7	1.1	3.0	3.2	8.1
26	0.424	31.0(0.5)	0.99(0.08)	45.4(3.7)	88.8	1.0	3.1	3.2	8.1
27	0.436	31.4(0.5)	0.88(0.07)	48.1(4.0)	90.9	0.9	3.0	3.4	8.1
28	0.433	50.6(0.5)	1.00(0.08)	39.2(3.2)	74.5	1.3	3.0	3.2	8.1
29	0.430	71.1(0.5)	2.01(0.15)	17.3(1.4)	29.5	1.3	3.0	3.2	8.1
30	0.607	16.3(0.5)	1.94(0.15)	31.7(2.5)	63.2	1.4	3.0	3.1	8.1
31	0.620	31.1(0.5)	0.98(0.08)	57.9(4.8)	100.1	0.9	3.1	3.4	8.2
32	0.621	52.7(0.5)	1.14(0.09)	48.9(3.9)	82.9	0.8	3.1	3.1	8.1
33	0.688	71.2(0.5)	1.64(0.13)	27.1(2.1)	35.4	1.3	3.1	3.1	8.1
34	0.905	16.3(0.5)	1.89(0.15)	36.9(2.9)	64.7	1.3	3.0	3.1	8.1
35	0.876	31.1(0.5)	0.90(0.07)	72.4(6.0)	119.6	0.8	3.0	3.4	8.1
36	0.907	52.7(0.5)	1.09(0.08)	66.3(5.2)	101.7	0.8	3.0	3.1	8.0
37	0.902	71.2(0.5)	1.62(0.12)	34.9(2.8)	40.6	1.1	3.0	3.1	8.1
$T = 300 \pm 3$ K									
38	0.204	31.4(0.5)	1.23(0.10)	28.2(2.3)	91.4	1.7	3.4	3.5	8.5
39	0.303	17.9(0.5)	2.13(0.16)	21.6(1.7)	67.2	1.1	3.3	3.1	8.1
40	0.302	36.1(0.5)	1.14(0.09)	36.7(3.0)	101.1	0.9	3.4	3.1	8.2
41	0.312	52.0(0.5)	1.27(0.10)	30.3(2.5)	78.7	1.0	3.2	3.1	8.1
42	0.312	68.8(0.5)	1.25(0.10)	21.4(1.7)	47.6	1.0	3.2	3.1	8.1
43	0.434	15.4(0.5)	0.97(0.07)	35.4(2.9)	59.3	0.9	3.2	3.1	8.1
44	0.411	31.0(0.5)	1.08(0.08)	43.7(3.6)	96.0	1.0	3.2	3.2	8.1
45	0.425	32.7(0.5)	0.95(0.07)	49.4(4.0)	99.9	0.7	3.3	3.1	8.1
46	0.443	35.0(1.0)	0.89(0.07)	53.6(4.4)	104.4	0.5	3.4	3.2	8.2
47	0.409	47.7(0.8)	0.97(0.07)	44.0(3.6)	89.3	0.7	3.4	3.1	8.1
48	0.411	68.5(0.5)	1.21(0.09)	27.7(2.2)	50.3	0.8	3.2	3.1	8.1
49	0.515	18.2(0.5)	1.95(0.15)	30.2(2.4)	74.5	1.1	3.7	3.1	8.3
50	0.518	35.2(0.5)	1.38(0.10)	46.8(3.8)	109.2	0.8	3.7	3.1	8.3
51	0.532	52.8(0.5)	1.01(0.08)	50.0(4.0)	92.8	0.7	3.6	3.1	8.2
52	0.787	33.0(1.0)	0.80(0.06)	76.8(6.3)	123.2	0.5	3.0	3.2	8.1
53	0.781	33.7(0.5)	1.19(0.09)	57.1(4.7)	118.4	1.1	3.1	3.5	8.3

made before filling the target and after evacuation of the mixture from it.

The chromatographical analysis showed the molecular compositions to be very close to the equilibrium ones,

$$C_{\mathrm{DD}} : C_{\mathrm{DT}} : C_{\mathrm{TT}} = C_d^2 : 2C_dC_t : C_t^2, \quad C_t + C_d = 1,$$

for each gaseous mixture exposed to a muon beam. However, for liquid mixtures, the molecular content can differ from the equilibrium due to the dynamic effects in

Continuation of Table 1

№	Conditions		ω, %	Y_n	Error contributions, %				
	φ, LHD	C_t, %			λ_c, μs^{-1}	Stat.	$\Delta\varphi$	Δq	Total
$T = 500 \pm 6$ K									
54	0.425	35.0(1.0)	0.88(0.07)	58.9(4.8)	130.0	0.6	3.1	3.2	8.2
$T = 550 \pm 6$ K									
55	0.201	33.7(0.5)	1.25(0.10)	30.2(2.5)	113.3	1.6	3.5	3.5	8.5
56	0.293	17.9(0.5)	1.92(0.15)	23.1(1.9)	73.5	1.1	3.5	3.1	8.2
57	0.285	36.1(0.5)	1.14(0.09)	42.8(3.5)	130.1	0.9	3.6	3.1	8.2
58	0.287	52.0(0.5)	1.07(0.08)	43.3(3.5)	135.6	0.9	3.5	3.1	8.2
59	0.292	68.8(0.5)	1.06(0.08)	38.7(3.1)	104.3	0.8	3.5	3.1	8.2
60	0.407	15.4(0.5)	0.93(0.07)	37.4(3.0)	66.1	0.9	3.4	3.2	8.2
61	0.399	32.7(0.5)	0.97(0.07)	35.4(2.9)	128.7	0.7	3.5	3.1	8.2
62	0.383	47.7(0.8)	0.87(0.07)	56.3(4.6)	133.1	0.7	3.6	3.1	8.2
63	0.390	68.5(0.5)	1.00(0.08)	45.8(3.7)	103.5	0.9	3.4	3.1	8.2
64	0.505	18.2(0.5)	1.81(0.14)	32.4(2.6)	79.8	1.1	3.8	3.1	8.4
65	0.490	35.2(0.5)	1.25(0.09)	50.3(4.1)	138.0	0.7	3.9	3.1	8.4
66	0.502	52.8(0.5)	0.93(0.07)	62.4(5.1)	141.8	1.2	3.8	3.1	8.4
67	0.604	51.5(0.5)	0.93(0.07)	68.0(5.5)	142.1	1.1	3.8	3.1	8.4
$T = 635 \pm 6$ K									
68	0.597	51.5(0.5)	0.94(0.07)	68.5(5.5)	155.5	0.5	4.0	3.1	8.4
$T = 800 \pm 10$ K									
69	0.191	33.7(0.5)	1.28(0.10)	36.2(3.0)	134.9	1.8	3.9	3.5	8.7
70	0.279	17.9(0.5)	1.88(0.14)	23.6(1.9)	78.8	1.2	4.3	3.1	8.6
71	0.275	36.1(0.5)	1.13(0.09)	40.2(3.3)	150.1	0.9	4.4	3.1	8.6
72	0.278	52.0(0.5)	1.16(0.09)	46.8(3.8)	165.2	0.8	4.0	3.1	8.4
73	0.278	68.8(0.5)	1.24(0.09)	39.7(3.2)	139.9	0.9	4.0	3.1	8.4
74	0.410	18.2(0.5)	1.93(0.15)	29.8(2.4)	84.5	1.0	4.0	3.1	8.5
75	0.400	35.0(0.5)	0.92(0.07)	60.2(4.9)	152.0	0.6	4.0	3.2	8.5
76	0.385	35.2(0.5)	1.50(0.11)	45.6(3.7)	150.3	1.0	4.3	3.1	8.6
77	0.405	51.5(0.5)	1.23(0.09)	51.9(4.2)	164.8	0.6	4.0	3.1	8.4
78	0.375	68.5(0.5)	1.25(0.09)	47.0(3.8)	145.0	0.8	3.9	3.1	8.4
79	0.484	18.2(0.5)	1.84(0.14)	32.7(2.6)	84.2	0.9	4.3	3.1	8.6
80	0.484	35.2(0.5)	1.29(0.10)	50.2(4.1)	155.3	0.7	4.3	3.1	8.6
81	0.491	51.5(0.5)	1.14(0.09)	59.4(4.8)	173.0	0.6	4.3	3.1	8.6

evaporation of a multi-component liquid, investigated by us under the conditions of our target in [54]. The deviation from the equilibrium state becomes noticeable for the high tritium concentration $C_t > 50\,\%$. Appropriate corrections to the molecular and isotope concentrations of the liquid mixture were made in [55]. We note that the quantity of protium in D/T mixtures did not exceed 1 %.

4.4. D/T mixture purity and ^{3}He accumulation

As follows from Eq. (10), the expression for the cycling rate is independent of the muon loss, including the effect of impurities with $Z > 1$. Contrary to this, the muon losses depend on the cycling rate ($\lambda_{dt\mu}$ and λ_{dt}). The larger the cycling rate, the closer the muon losses are to their natural limit equal to the probability ω_s.

As is seen from Eq. (11), the muon transfer to the possible impurities affects the value of ω. That is why the impurity level must be made as small as possible. Actually, the condition

$$\lambda_Z C_Z \ll \omega_s \lambda_c \tag{12}$$

must be ensured.

It is necessary to distinguish two sorts of impurities: impurities with $Z > 2$ and He admixtures.

4.4.1. Impurities with $Z > 2$ and ^{4}He

These impurities are predominant helium-4, carbon, oxygen, and nitrogen originating from imperfect purification of the mixture before filling the target and removing the residual gaseous elements from the target walls during the exposure.

The special preparation system based on palladium filters [46] provides filling of a target with gas purified of impurities at the level $C_Z < 10^{-7}$ of volume parts. As the outgassing effect increased with temperature, the mixture purity varied from $C_Z < 10^{-7}$ for $T = 20$ K to $C_Z = 10^{-5}-10^{-6}$ for $T = 800$ K. The rate of the muon transfer from the $t\mu$-atom to the pointed admixtures is $\lambda_Z \sim 10^{11}$ s^{-1} for nuclei with $Z > 2$ [56] and $\lambda_{^4\mathrm{He}} \sim (1\text{–}5) \cdot 10^9$ s^{-1} for ^{4}He [57, 58]. Therefore, condition (12) is satisfied only for a liquid D/T mixture where the cycling rate is rather high ($\lambda_c = 50\text{–}120$ μs^{-1} depending on the tritium concentration) and most impurities (excluding helium) are solid and freezed out on the target walls.

4.4.2. ^{3}He admixture

The tritium handling system provides the initial concentration C_{He} of ^{3}He in the mixture before pouring into a target at the level 10^{-7}. However, due to the tritium β-decay, ^{3}He is accumulated in a target according to relation

$$C_{\mathrm{He}}(\tau) = C_t[1 - \exp(-\lambda_{trit}\tau)],$$

where $\lambda_{trit} = 6.4 \cdot 10^{-6}$ h^{-1} is the tritium decay rate. Hence, the process of the muon transfer from the $t\mu$-atom to ^{3}He (with the rate $\lambda_{^3\mathrm{He}} \approx 2 \cdot 10^8$ s^{-1} [57]) can essentially affect the muon losses.

The ^{3}He accumulation effect is quite different for liquid and gaseous D/T. It was shown in experiment [58] that ^{3}He in liquid D/T diffuses and goes out to the vapor gas. Our cooling system of the LTT [43] provided the passage of all the D/T mixture through the vapor phase during approximately 1 hour, which led to the ^{3}He escape out of liquid D/T. In experiments with liquid D/T, we therefore had no problem with D/T purity.

In experiments with gaseous D/T, we were forced to refill the target every 10–40 hours (depending on the tritium content in D/T) to avoid accumulation of ^{3}He larger than the «critical value» $C_{^3\mathrm{He}} \approx 10^{-5}$.

5. DATA TREATMENT

The data processing included the following stages.

1. Selection of events. By an event we mean an occurrence of the processes caused by a single muon beginning with the muon stop in the target and ending with the muon decay. An example of the event as seen by the detectors is presented in Fig. 7. The most important criteria for the event to be accepted was presence of a reliable signal for the μ-decay electron.

2. Creation of the charge and time spectra for neutrons from the $d+t$ reaction and for electrons from the μ-decay.

3. Fit of these spectra to determine the «effective» MCF parameters λ_c, ω, and Y_n.

4. Analysis of these parameters as functions of the tritium concentration to obtain the $dt\mu$ formation rates $\lambda_{dt\mu-d}$ and $\lambda_{dt\mu-t}$ and the muon-to-helium sticking probability ω_s.

5.1. Analysis methods

The most popular and practically the only method used by most groups involved in the study of the MCF $d+t$ process is the so-called standard method, where the yield and time distribution of all detected neutrons from reactions (5), (6) are registered and analyzed. This distribution has the well-known one-exponent form (8). The number of μ-decay electrons N_e is used for normalization,

$$\frac{N_n}{N_e} = \frac{\epsilon_n \Lambda_c}{\lambda_0 + \omega \Lambda_c}. \tag{13}$$

The slope λ_n of the exponential in (8) and the normalized neutron yield Y_n are the measured parameters. The values of Λ_c, ω, and Y_n are extracted from (8), (9), and (13):

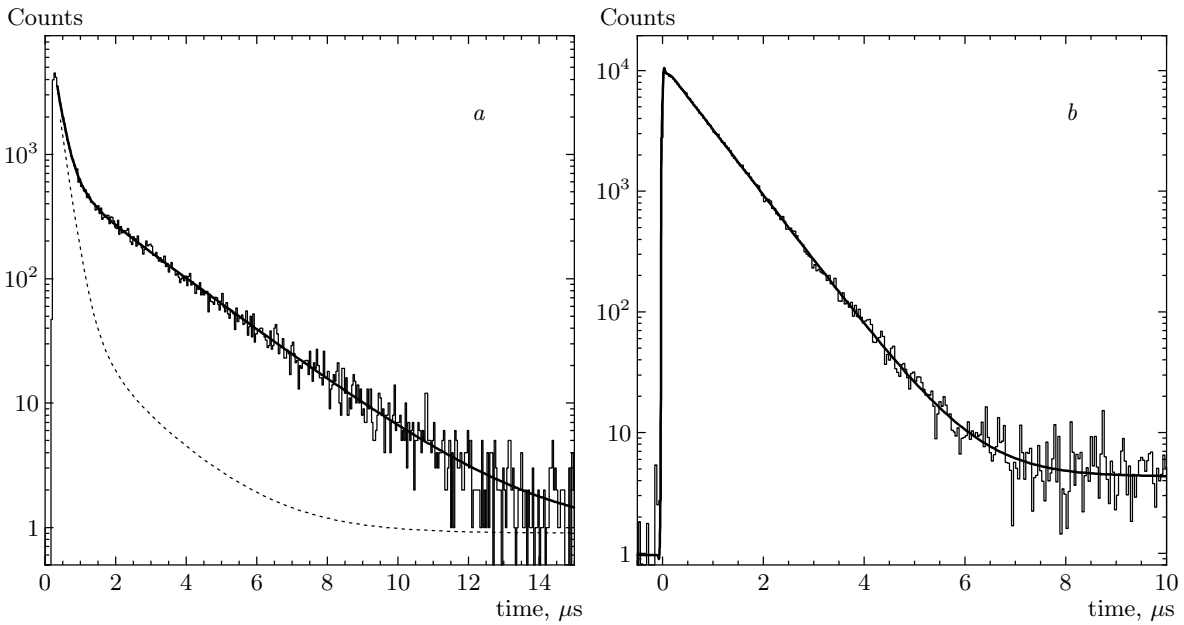

Fig. 8. Example of electron (a) and neutron (b) time distributions. Solid lines are the optimum fits with expressions (15) (a) and (8) (b), the dashed line corresponds to the electrons from empty target

$$\epsilon_n \varphi \lambda_c = \frac{N_n}{N_e}\lambda_n, \quad \frac{\omega}{\epsilon_n} = \frac{\lambda_n - \lambda_0}{\epsilon_n \varphi \lambda_c}, \quad \epsilon_n Y_n = \frac{N_n}{N_e}. \quad (14)$$

In the Dubna experiments, we also used the standard method. To obtain spectrum (8), we created a time distribution of the neutron detector charge $Q(t)$. For this, we summed the amplitude spectra for each neutron detector *ND1* and *ND2*. Then the spectrum $Q(t)$ was transformed to the time distribution of the number of events

$$N_n(t) = Q(t)/\overline{q}$$

using the unit charge $\overline{q}$ [59]. The latter was measured under special conditions providing a low neutron multiplicity, where each charge pulse corresponded to one neutron. Charge distributions obtained in such exposures were compared with the calculated ones to obtain the experimental value of ϵ_n as a function of the threshold.

The number of electrons N_e was obtained from the analysis of the electron time spectra $N_e(t)$ using the distribution $B_{empty}(t)$ measured with an empty target,

$$N_e^{total}(t) = kB_{empty}(t) + A_e \exp(-\lambda_e t) + F, \quad (15)$$

where λ_e is the muon disappearance rate and F is the accidental background. In this fit k, A_e, λ_e, and F are parameters. The observed muon disappearance rates λ_e are close to the muon decay rate $\lambda_0 = 0.455\ \mu s^{-1}$ and depend on the mixture purity. In exposures with liquid D/T, where the purity is maximum, λ_e is obtained equal to λ_0 within 1 %.

A typical example of the fitted time distributions of decay electrons and fusion neutrons for the D/T filled target is shown in Fig. 8. The dashed line corresponds to the electrons from decays of muons stopped in the target walls (empty target).

The principal disadvantage of the standard method is that the main MCF parameters — cycling rate and effective muon losses — are not obtained directly, only their product is measured directly. In our measurements, we employed two novel independent methods proposed and developed in Dubna [60, 61]. These analysis methods make it possible to directly measure the values of λ_c and ω.

A proposal in [60] was to measure the distribution $N_{ne}(t)$ which was a function of the interval $t = t_e - t_n$ between the last detected neutron of the series and the μ-decay electron. This distribution has the form of a sum of two exponentials with significantly different slopes [60, 61],

$$\frac{dN_{ne}}{dt} = \frac{\lambda_0}{\lambda_n} \times$$
$$\times[\omega\Lambda_c \exp(-\lambda_0 t) + \epsilon_n \Lambda_c (1-\omega) \exp(-(\lambda_0+\lambda_n)t)], \quad (16)$$

where λ_n is expressed as

$$\lambda_n = (\epsilon_n + \omega - \epsilon_n \omega)\Lambda_c. \quad (17)$$

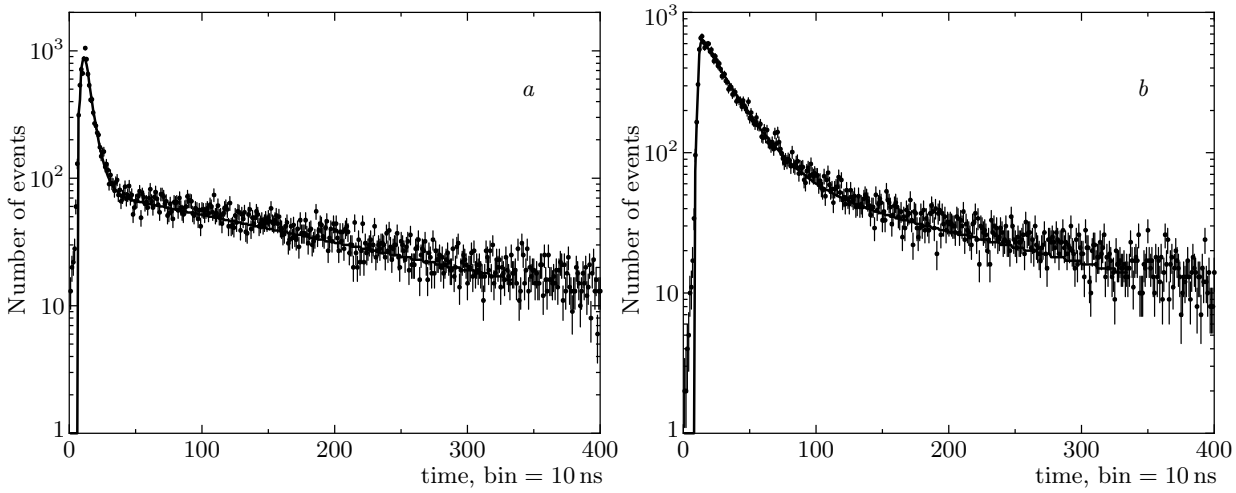

Fig. 9. Electron – last neutron timing spectra measured with a liquid D/T mixture. Spectrum a corresponds to the exposure with $C_t = 35.2\,\%$ and variant b was selected for $C_t = 85.5\,\%$. Lines are the fits with expressions (16) and (17) and the optimum parameters $\epsilon_n\Lambda_c$ and ω/ϵ_n

The first («slow») exponential corresponds to the events with muon sticking and the second («fast») one to the events without sticking. The cycling rate is determined from the fast component slope, and the muon loss is obtained from the ratio between the amplitudes of the slow and fast exponentials:

$$\frac{A_s}{A_f} = \frac{\omega}{\epsilon_n(1-\omega)}.$$

Examples of such distributions obtained in a liquid D/T mixture are presented in Fig. 9. As is seen from the figures, the events with and without sticking are clearly separated. Different slopes of the fast components of the spectra reflects the different values of the cycling rate realized for the tritium concentrations $C_t = 35.2\,\%$ and $C_t = 85.5\,\%$. The advantage of the method is that charge calibration is not necessary in this case.

Another idea [61] was to measure the neutron multiplicity distribution (the number k of detected neutrons per muon) in some definite time interval T. If one selects the events for which the muon does not decay in this interval, then this distribution is a sum of two terms. One of them, which is Gaussian (Poisson) with the mean $m = \epsilon_n\Lambda_c T$, corresponds to the events without sticking, and the other, depending on ω and falling with k, is the distribution of events with muon sticking.

The rigorous expression for the multiplicity distribution was obtained in [62]. It has the form

$$f(k) = \frac{[\epsilon_n(1-\omega)]^k}{(\epsilon_n+\omega-\epsilon_n\omega)^k}P(k) + \frac{[\epsilon_n(1-\omega)]^{k-1}\omega}{(\epsilon_n+\omega-\epsilon_n\omega)^k}F(k), \quad (18)$$

where $P(k)$ is the Poisson distribution with the mean $m = \lambda_n T$,

$$P(m) = \frac{(\lambda_n T)^k}{k!}e^{-\lambda_n T},$$

$$F(k) = 1 - e^{-\lambda_n T}\sum_{i=0}^{k-1}\frac{(\lambda_n T)^i}{i!},$$

and λ_n is given by formula (17).

Formula (18) corresponds to the «event mode» where the number of detected neutrons was considered. Actually measured in experiments were the distributions of the neutron detector charge; they were divided by the unit charge to obtain a multiplicity distribution. The real response function of the detector results in diffusion of the measured spectra as compared with the ones obtained in the «event mode». It turns out that in good approximation (with accuracy 2–3 % in cycling rate), the real distribution can be obtained as convolution of formula (18) with the Gaussian function. The Gaussian width is varied to obtain the best agreement between the experiment and calculations.

We can also select only nonsticking events. For this, we must exclude the requirement of the electron signal in the trigger and select only those neutron series whose duration is larger than the chosen interval T. Plotting and analyzing the multiplicity distribution of such events, we can directly obtain the cycling rate.

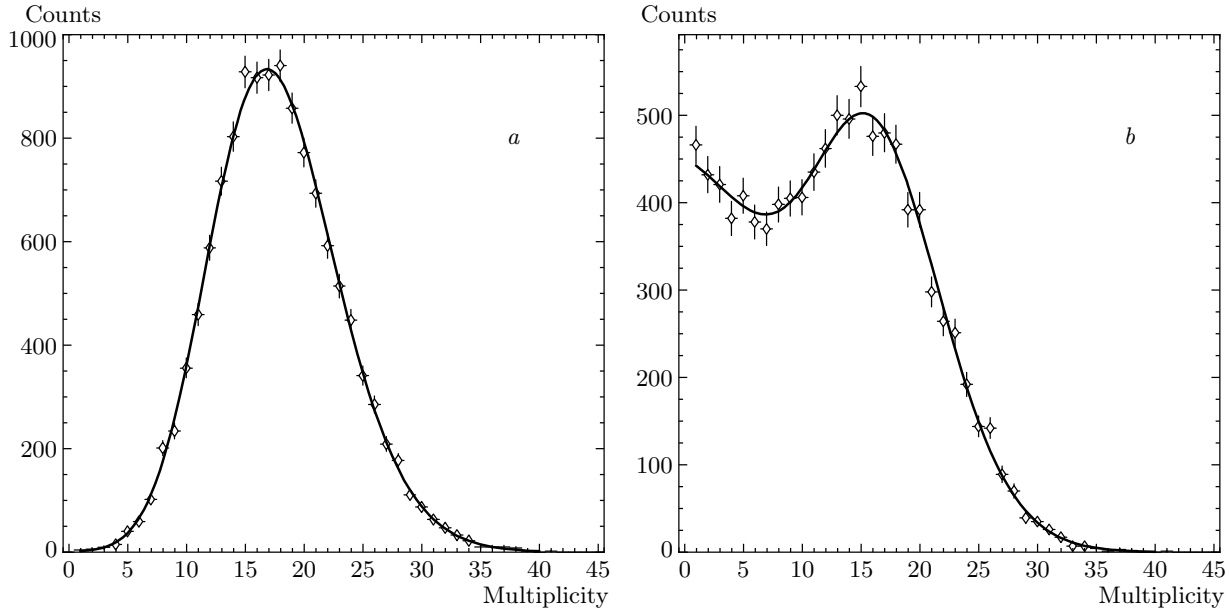

Fig. 10. Multiplicity distributions in time interval $T = 1$ μs. a — Distribution without sticking events, b — with sticking events. Curves are the optimum fits

The advantage of this method is that we do not need the fact of the μ-decay electron existence. Of course, only λ_c can be determined in this case because events without muon sticking to helium are accepted. The examples of fitted multiplicity distributions are presented in Fig. 10.

The comparison of all methods that we used in the analysis is given in the Table 2. The statistical power is practically the same for all methods. Indeed, in the standard method, the main factor for the statistical accuracy is the limited number of electrons, the number of neutrons is much higher under real experimental conditions. In two other methods, the full statistics is the number of the first or last neutrons, which are also approximately equal to the electron number.

In our investigations, we use all the three methods mentioned. This allows us to reliably analyze the data, with minimum systematic uncertainties. Of course, the full analysis is rather complicated and includes many tests with different selection rules for events to be accepted.

5.2. Electron identification

A serious problem in the MCF data analysis is how to distinguish the real electron from a false one. Under the conditions where one muon can cause up to 100 reactions (5), it is possible to detect a neutron by the electron detector and accept it as an electron. Contrary to the measurements of other groups, we detect electrons with a proportional wire counter, having a very low sensitivity to neutrons. But even in this case, the fraction of false electrons caused by the neutron counts was noticeable.

Only the last (in time) electron signal is accepted as real. It would be enough to exclude the false electrons if the electron detection efficiency would be $\epsilon_e = 100\,\%$. However, for different reasons (see [63]), this efficiency is not equal to unity. Thus, the situation can occur where the real electron is not detected and a false one is interpreted as real. The presence of false electrons results in distortion of λ_c, ω, and Y_n. The cycling rate determined according to formula (14) is distorted due to the error in N_n and N_e, and λ_n extracted from expressions (8) and (15) feels the error in λ_c. On the other hand, confusion of the real and false electrons leads to distortion in the relation between «stick» series (interrupted due to the muon sticking) and «no-stick» series (ending with μ-decay). The latter are accepted more effectively. Thus, the results for the muon losses are also distorted. Finally, the distortion of the slope of the electron time distribution does not make it possible to correct the estimate of the D/T mixture purity, and thus to check the parameters of the purification system.

Fortunately, the cycling rate determined from the peak position in the multiplicity spectrum is free of

Table 2. Comparison of different methods used in the MCF study

Method	λ_c, ω determination	Charge calibration	Electron detection
Standard	Indirect	Necessary	Necessary
t_e–t_n	Direct	Not necessary	Necessary
Multiplicity	Direct	Necessary	Not necessary

false electrons. This is a very important circumstance allowing reliable data on the cycling rate serving as a source of the «elementary» process parameters such as the $dt\mu$-molecule formation rate. Of course, it is very desirable to obtain a correct value for λ_c by different independent methods. Moreover, obtaining correct data on the muon losses is an independent important task.

5.2.1. Selection by the energy loss in the neutron detector

The effective way to reject false electrons was elaborated and used in our work [23]. For this, we required the following when selecting events.

1. Electron signals from the PC and *ND1* or *ND2* should coincide.

2. The energy that the electron releases in the neutron detector should be greater than the maximum possible energy released by a 14 MeV neutron in this detector. This allows reliable discrimination of false electrons. The use of these selection criteria allowed us to obtain the data on λ_c and ω coinciding for all three analysis methods within 5 % [23].

The disadvantage of this selection is a decrease in the statistics because an essential part of the useful events are rejected. This decrease becomes much more sensible in experiments with a high-pressure gaseous target having rather thick walls, for which the «output» electron energy spectra are noticeably distorted and the transparency of the target walls for electrons is noticeably smaller than for the liquid target. Therefore for a gaseous target, reliable neutron–electron separation was connected with larger statistics losses than for a liquid target.

5.2.2. Selection by the time position of the electron signal relative to neutron series

To avoid losing statistics, we developed a new method [63] for the false electron discrimination, which is most effective for the large neutron detection efficiency realized in our experiments. We now impose the criterion «electron inside neutron series». For this, we consider the neutron detector charge Q (the sum of the amplitudes) on some time interval (ΔT) close to the electron signal and delayed relative to it by Δt. The events were accepted under the condition that the charge Q is smaller than the threshold: $Q < Q_{th}$. Our consideration [63] shows that the proper values are $\Delta t = 60$ ns and $\Delta T = 500$ ns. The largest values of Q_{th} correspond to events without selection for the false electron. In this case, the distortion in the electron yield and time spectrum (15) is the largest. The opposite case (low Q_{th}) corresponds to the smallest distortions for electrons and to the minimum value of the electron time slope λ_e, which practically coincides with the one determined using selection by electron energy in the neutron detector.

The opposite situation occurs for the slope of neutron time distribution (8). In the case where the real electron is not detected, a false one is accepted as electron. This means that the long neutron series are predominantly detected because the appearance of a false electron is most probable just in those series. Indeed, our considerations [63] show that the minimum Q_{th} (maximum false electron rejection) leads to the maximum slope λ_n. Again, the «correct» value of λ_n is in agreement with the one obtained with selection by electron energy in the neutron detector.

The main MCF parameters obtained under two different selection options coincide within the accuracy 3–4 %. The reliability of the data is confirmed by the fact that the value of the cycling rate determined by the standard method is identical to the one yielded by the multiplicity method, where it is independent of the selection criteria. The method considered gives the statistics 4–5 times larger than in the case with energy discrimination (Sec. 5.2.1). This indicates that we have found the way described in detail in [63] for correctly obtaining the MCF parameters without essential loss in statistics.

5.3. Neutron detection efficiency

All methods discussed above give the values of $\lambda_c\epsilon_n$ and ω/ϵ_n. To obtain the MCF parameters λ_c and ω, we must know the neutron detection efficiency ϵ_n.

Determining ϵ_n for organic scintillation counters is a nontrivial task because it is influenced by factors like the geometry of the surrounding material, generation of light by various reaction products and because many energy-dependent cross sections are involved. Because of the lack of neutron calibration sources with well-known intensity and sufficiently large energy, the efficiency had to be calculated. The Monte Carlo technique was used.

Calculations of ϵ_n for neutrons detected by the ND in the Dubna experiments are described in [64]. The CERN package GEANT was used in [64] for the simulation calculations. Because it lacks the appropriate low and fast neutron interaction cross sections, GEANT was linked with the MICAP package. MICAP uses experimental neutron cross sections from the ENDF/B-VI database from 20 MeV down to thermal energies (10^{-5} eV). This includes partial cross sections, angular distributions, and energy distributions of reaction products and de-excitation photons. The preprocessed ENDF/B-VI data represent the experimental data within 2 %.

After the calculation of the energy deposited inside the scintillator, the electronic output signal was obtained by first converting the energy into scintillation light considering the particle type, and then converting the total light output into an electric signal by applying the detector response function [49]. This function takes several factors into account, such as nonuniform light collection depending on the position of light generation inside the scintillator and photon statistics. The results of calculations [64] for 14 MeV neutrons from reactions (5), (6) are presented in Fig. 11 together with the measured spectra.

One neutron detected in a scintillator may generate a response from one detector or, due to scattering or to generated gamma rays, from both detectors. This leads to a single and coincident rate. The corresponding spectra are shown in Fig. 11 together with the measured ones. As can be seen, there is good agreement between the measurements and the calculations in both cases (single and coincident). The intensity and amplitude calibration of the calculated single spectrum was normalized to single data. The normalization thus obtained is then applied to the calculated coincident spectrum, which then neatly coincides with the corresponding data. This means that the single-to-coincident ratio is well predicted, which is considered as a sensitive validation check for the calculations. The estimated relative uncertainty in ϵ_n is not worse than 5–7 %.

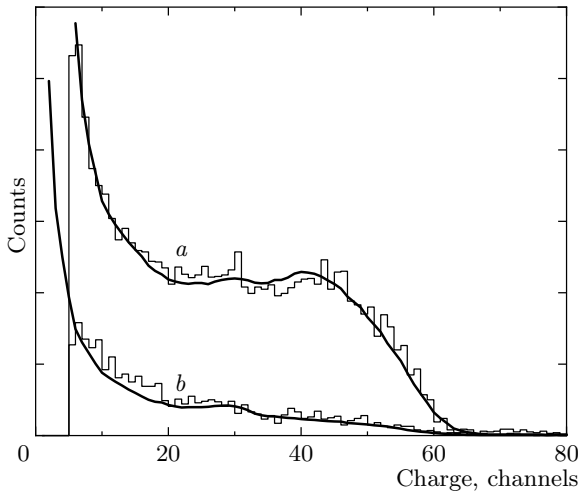

Fig. 11. Charge distribution for 14 MeV neutrons measured in [23] with the ND (histograms). Distributions are plotted for single (a) and coincident (b) events. Lines are the Monte-Carlo calculations [64]

The problem is how the neutron detection efficiency depends on the neutron multiplicity (cycling rate). The main idea of using the flash ADC is that the total charge per number of neutrons is conserved even when the ND signals mostly overlap. However, it is true only for zero charge threshold. In fact, the cluster charge should be limited to reduce the low-energy background. At a high neutron multiplicity, small-charge clusters can overlap with one or more other clusters and hence can be accepted (a noneffective threshold). Obviously, this results in an increase of the detection efficiency compared with the low neutron multiplicity. The actual increase depends on several factors, such as the shape of the ND signal, the form of the response function, the magnitude of the threshold, and the measured cycling rate. Because one would expect an essential correction to the value of ϵ_n, the problem required special consideration.

This was made in [65], where the fusion neutron registration was Monte-Carlo simulated for a wide cycling rate. All the three analysis methods were considered. It turned out that in the standard and multiplicity methods, the corresponding corrections to the efficiency were not very large: even for the maximum possible measured cycling rate $\epsilon_n\Lambda_c = 40\ \mu\text{s}^{-1}$, they are only 12 %.

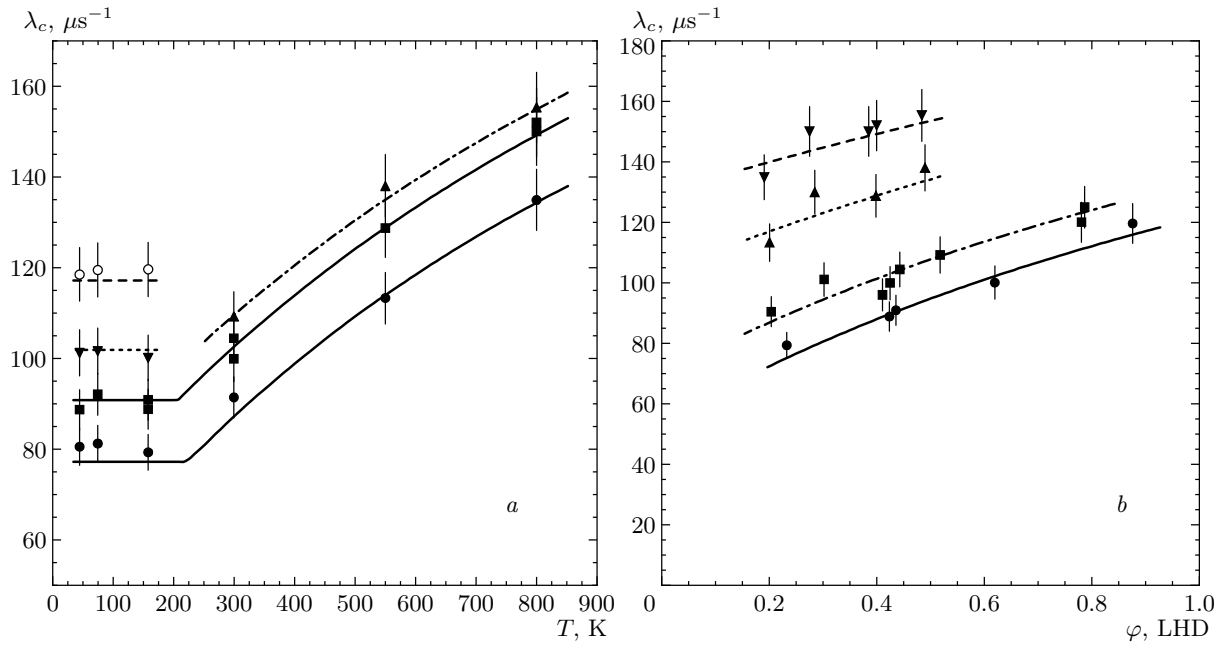

Fig. 12. a — Normalized cycling rates as a function of temperature for the gaseous D/T mixture at $C_t \approx 33\,\%$ and different densities $\varphi = 0.88$–0.91 (○), 0.62–0.64 (▼), 0.49–0.52 (▲), 0.39–0.45 (■), 0.19–0.24 (●) LHD. b — Normalized cycling rates as a function of density for the gaseous D/T mixture at $C_t \approx 33\,\%$ and different temperatures $T = 800$ K, $C_t = 0.34$–0.36 (▼); $T = 550$ K, $C_t = 0.33$–0.36 (▲); $T = 300$ K, $C_t = 0.31$–0.36 (■); $T = 158$ K, $C_t = 0.31$ (●). The curves are obtained with optimum parameters

6. RESULTS

6.1. The effective MCF parameters

The effective MCF parameters λ_c, ω, and Y_n were obtained from the fit of the distributions considered in the «standard», «multiplicity», and «$t_e - t_n$» analysis methods. Although the first two methods are more reliable, the results obtained by three different methods were in agreement with an accuracy 3–4 %. They are presented in Table 1 and in Fig. 12.

The statistical uncertainty in the results is determined by the number of events and the fit accuracy. In both main methods («standard» and «multiplicity»), the statistics provides this error not higher than 2 %. We note that in the multiplicity method, we do not need the muon number normalization.

The following factors contribute to the systematic error.

1. Uncertainty in the neutron detection efficiency makes the maximum contribution to the systematic error. It was estimated from the calculation of ϵ_n and the accuracy in the energy threshold determination and is 6 % in total.

2. Uncertainty of the charge calibration procedure gives an error smaller than 3 %.

3. Uncertainty of the gas and liquid density (for normalized cycling rate) is about 3–4 % and 2 % respectively.

4. Uncertainty of the time zero position (only for the standard method) gives a systematic error smaller than 0.5 %.

5. Uncertainty due to the correct selection of muon decay electrons (only for the standard method, see Sec. 5.2) is 2 %.

6. Uncertainty caused by possible instability of detectors and electronics does not exceed 2 %.

Therefore, the total uncertainty in ω, Y_n, and the absolute values of λ_c did not exceed 9 %. Obviously, the relative dependencies of the cycling rate on temperature and density are known with a better accuracy (4.5–5.5 %).

6.2. The $dt\mu$-molecule formation rate and muon sticking probability

The usual way to determine the «physical» values $\lambda_{dt\mu}$ and ω_s is an analysis of the «effective» parameters λ_c and ω using expressions (10) and (11), representing their dependence on tritium concentration and density. For this purpose, it is first of all necessary to express

q_{1S} as a function of C_t and φ. With the general expression (1) and the theoretical predictions in [32, 34, 66] as well as experimental results in [17, 35] taken into account, the parameterization of q_{1S} was chosen in the form

$$q_{1S}(C_t, \varphi) = \frac{1}{1 + (b + c\varphi)C_t}. \qquad (19)$$

6.2.1. Fit of the liquid D/T data. Muon sticking probability ω_s

As we have noted, the most expedient condition for the ω_s measurement is a liquid D/T mixture, where λ_c is high and the admixture content is negligible. Our first data for the liquid D/T mixture were given in [23]. In this paper, we correct the values of the molecular concentrations and in addition perform the common fit of λ_c and ω in liquid D/T using formulas (10) and (11). As for all liquid points, the density values were very close to each other, the parameterization for q_{1S} was chosen as

$$q_{1S}(C_t) = (1 + aC_t)^{-1}, \qquad (20)$$

where $a \equiv b + c\varphi$ from (19). We have performed a set of fits, varying different parameters according to the known theoretical and experimental data for λ_{1-0} [68, 69], $\lambda_{tt\mu}$ [70–72], and $\lambda_{dt\mu-t}$ [14, 17, 18, 70]. Such a variation does not lead to a significant change in the results. The systematic error $\Delta\epsilon_n$ (the same for all liquid data) was excluded from the data errors in this fits. In Table 3, the values used for the MCF cycle parameters and the results of one of the fits are shown.

The fit results are shown in Fig. 13 and in Table 3. The main results for the liquid ($T \approx 22$ K, $\varphi \approx 1.22$ LHD) D/T mixture are

$$\lambda_{dt\mu-d} = (685 \pm 35^{stat} \pm 41^{syst})\ \mu\text{s}^{-1}, \qquad (21)$$

$$\lambda_{dt\mu-t} = (18 \pm 6^{stat} \pm 11^{syst})\ \mu\text{s}^{-1}, \qquad (22)$$

$$\omega_s = (0.573 \pm 0.021^{stat} \pm 0.032^{syst})\,\%\,. \qquad (23)$$

Our value of $\lambda_{dt\mu-d}$ in (21) is essentially higher than the PSI group data [14] but is in agreement with the LAMPF results [17] (see Fig. 15). The value of $\lambda_{dt\mu-t}$ in (22) is in satisfactory agreement with the values obtained in [17, 18], $\lambda_{dt\mu-t} = 20\ \mu\text{s}^{-1}$, and [70], $\lambda_{dt\mu-t} = 11^{+6}_{-11}\ \mu\text{s}^{-1}$. An unexpectedly high rate $\lambda_{dt\mu-t} = 160\ \mu\text{s}^{-1}$ was obtained by the RIKEN group [16, 73]. Fixing this value, we do not achieve any satisfactory agreement of fit to our data, and we therefore conclude that this value is uprated by about a factor of 5.

Table 3. Results of one from the set of common fits of the data for liquid D/T. Fixed parameters are given with references

Parameter	Value	Ref.
a	2.9 ± 0.4	free
$\lambda_Z C_Z$, μs^{-1}	0.08 ± 0.03	free
λ_{dt}, μs^{-1}	280	[18, 21, 35, 36]
λ_{1-0}, μs^{-1}	1200	[68, 69]
$\lambda^{3/2}_{dd\mu}$, μs^{-1}	3.5	[11]
$\lambda_{3/2-1/2}$, μs^{-1}	36	[11]
λ^{tt}_f, μs^{-1}	14	[72]
ω_{dd}, %	0.13	[11]
r	0.51	[11]
$\lambda_{tt\mu}\omega_{tt}$, μs^{-1}	0.28 ± 0.15	free
$\lambda_{dt\mu-d}$, μs^{-1}	650 ± 40	free
$\lambda_{dt\mu-t}$, μs^{-1}	21 ± 8	free
ω_s, %	0.574 ± 0.022	free

The probability ω_s of the effective muon-to-helium sticking in dt-fusion is one of the most important MCF characteristics because it limits the number of fusions per muon. In theory, ω_s is considered as the product

$$\omega_s = \omega_s^0(1 - R),$$

where ω_s^0 is the «initial» sticking probability directly after fusion and R is the probability of the muon-from-helium stripping during the Heμ thermalization stage. R is density-dependent and hence the theory predicts a slow, close to linear, decrease of ω_s with density. Comparison of different theoretical and experimental results on ω_s is presented in Table 4.

The mean value $\lambda_Z C_Z = 0.08 \pm 0.03\ \mu\text{s}^{-1}$ obtained in the fits is in agreement with the estimate $0.08 \pm 0.04\ \mu\text{s}^{-1}$ based on the analysis of the electron time spectra. The product $\lambda_{tt\mu}\omega_{tt}$, being free, was obtained as 0.28 ± 0.15, which agrees with [70–72].

6.2.2. Low-temperature gaseous D/T data

Here, we present new data related to the mixture temperature $T = 45$, 158 K and different densi-

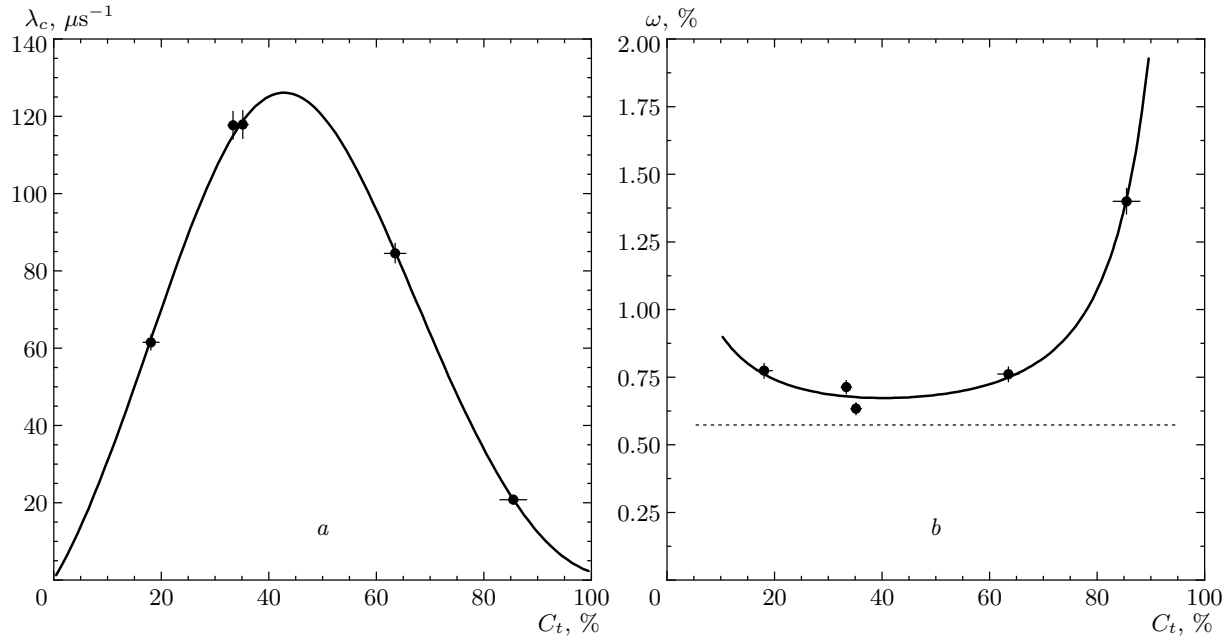

Fig. 13. Normalized cycling rates (a) and muon loss probability (b) as a function of the tritium concentration for the liquid D/T mixture ($T = 22$ K, $\varphi \approx 1.22$ LHD). Solid lines are optimum fits. The dashed line is the value (23)

ties $\varphi = 0.2$–1 LHD. It is primarily interesting from the standpoint of the density dependence of the $dt\mu$-molecule formation rate on D_2 molecules.

For all values of φ, approximation (20) for q_{1S} was used in the fit. The results are presented in Table 5. The data for $T = 300$ K recently presented in [26] is also included. As can be seen, the obtained data for $\lambda_{dt\mu-d}$ demonstrate a strong density dependence and practically do not sensitivity to the mixture temperature.

6.2.3. High-temperature gaseous D/T data

Measurements for high temperatures ($T \geq 300$ K) are important for the determination of the $dt\mu$-molecule formation rate on DT molecules. According to the «standard» theory, the Maxwell distribution for the $t\mu$-energy ($E_{t\mu}$) overlaps the nearest resonance $\lambda_{dt\mu-t}$ ($E_{t\mu}$) in this region. In addition, it is interesting to clarify for which temperatures $\lambda_{dt\mu-d}$ remains density-dependent and what is its temperature dependence.

The preliminary data for $T = 300$, 550, 800 K were presented in [26]. We now present the final data obtained from the common fit of the experimental dependences λ_c (φ, T). The $dt\mu$-molecule formation rates on D_2 and DT molecules were assumed independent of density at temperatures $T > 300$ K. They are presented in Table 6.

The following conclusions can be made from their consideration.

1. According to theory, $\lambda_{dt\mu-t}$ rises with temperature.

2. Contrarily this, $\lambda_{dt\mu-d}$ does not reveal a temperature dependence.

6.2.4. Common fit of gaseous D/T data

To reliably extract $\lambda_{dt\mu}$ for given T and φ, each set of $\lambda_c(\varphi, T; C_t)$ should contain enough points corresponding to a wide range of C_t. Not all our data satisfied this condition. We could not conduct measurements with high C_t at «extreme» φ and T. Nevertheless, we could include all data in the analysis making some assumptions on the $\lambda_{dt\mu}$ density and temperature dependences.

Based on our preliminary analysis [26, 67] and temperature and density dependences of λ_c obtained from the analysis of the total data, we can conclude that

(i) $\lambda_{dt\mu-d}$ rises linearly with density in a wide temperature range up to $T = 300$ K;

(ii) at temperatures $T = 300$–800 K, $\lambda_{dt\mu-t}$ is very close to a linear function of temperature and does not depend on density.

We therefore chose the simplest linear parameterization for the temperature and density dependences of the formation rates:

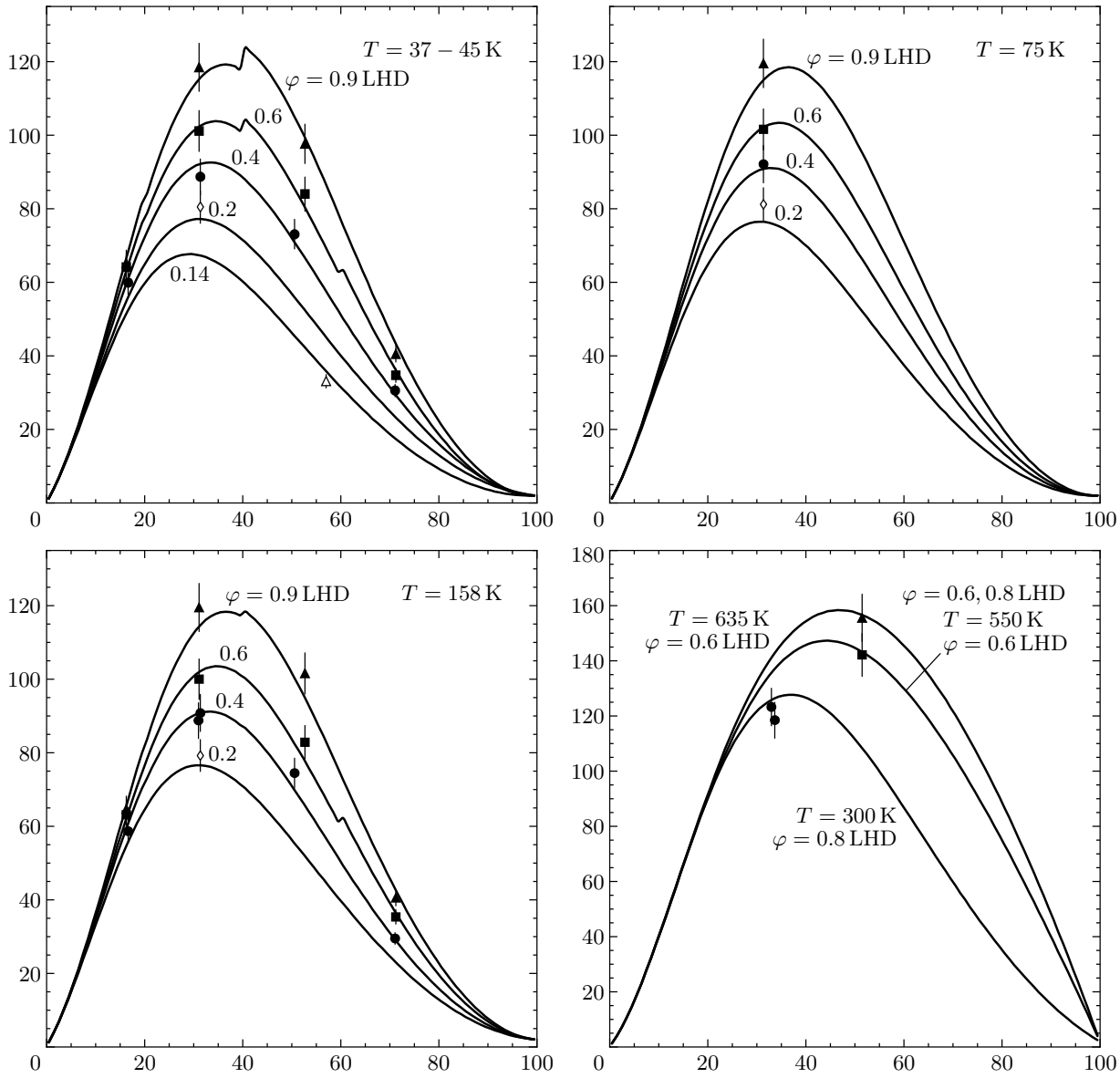

Fig. 14. Common fit of the normalized cycling rates as a function of the tritium concentration for all (76 points) data for the gaseous D/T mixture ($T = 37$–800 K, $\varphi = 0.143$–1.024 LHD). Lines are the optimum fit

$$\lambda_{dt\mu-d}(\varphi) = A_d + B_d\varphi \quad \text{at} \quad T = 37\text{–}300\ \text{K};$$
$$\lambda_{dt\mu-d} = C_d \quad \text{at} \quad T > 300\,\text{K}, \tag{24}$$

$$\lambda_{dt\mu-t}(T) = A_t + B_t T \quad \text{at} \quad T \geq 200\ \text{K},$$
$$\varphi = 0.2\text{–}0.9. \tag{25}$$

The general expression (19) was used for q_{1S}, including the density-dependence term.

A total of 76 gaseous points of λ_c were under fitting by using formula (10). The systematic error due to the neutron detection efficiency $\Delta\epsilon_n$ (the same for all data) was excluded from the errors in the course of fitting. The results are presented in Table 6 and Figs. 14–16.

Figure 14 shows how the experimental values of λ_c are described by formulas (10) with our parameterization of q_{1S} and $\lambda_{dt\mu}$. It follows from the fit that the experimental data are in satisfactory agreement with the used approximation: $\chi^2 = 84$ for 76 points and 6 variable parameters. The optimum values of our approximation are presented in Table 7. We note that q_{1S} turned out to be density-independent. The same was

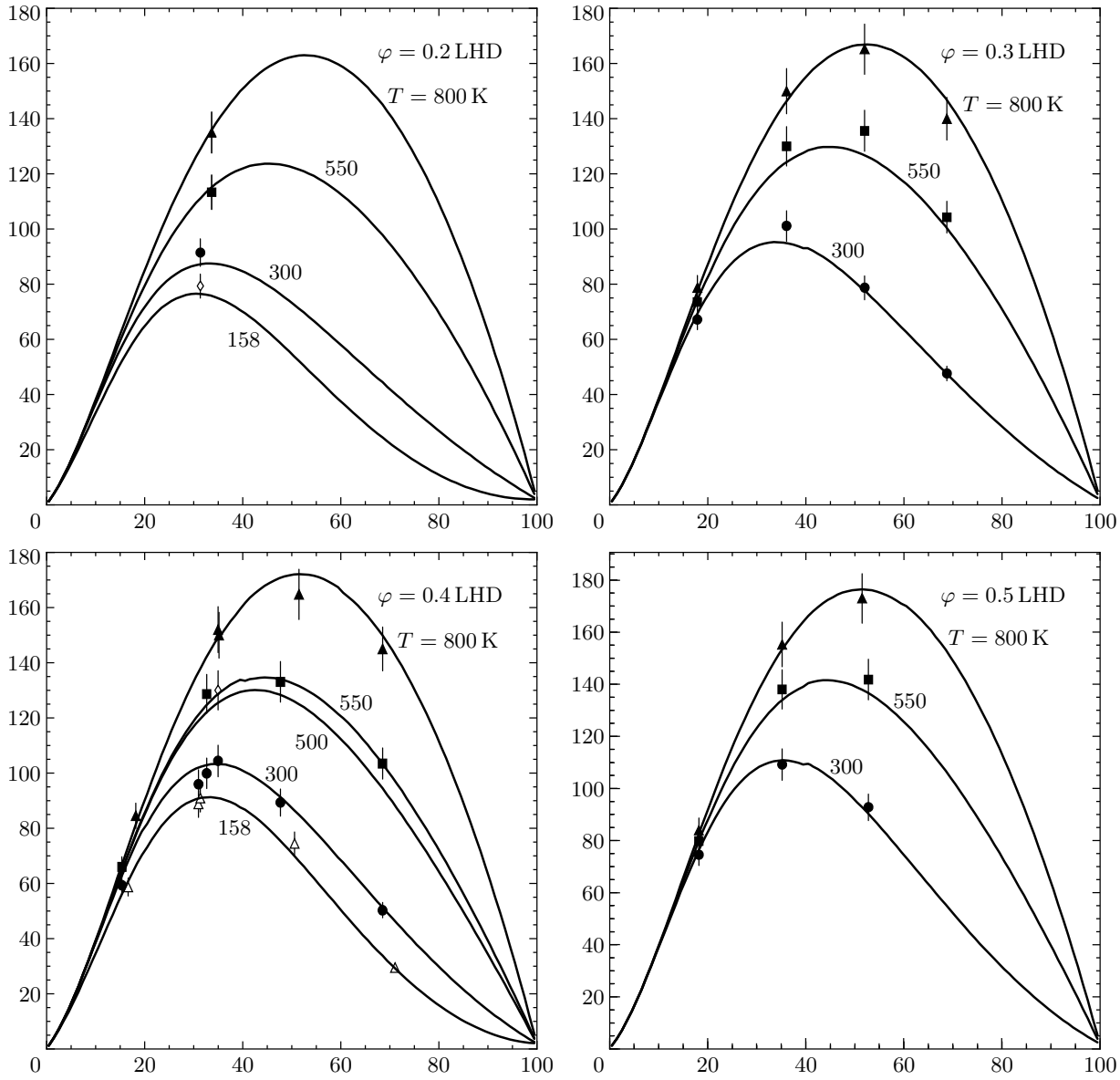

Fig. 14.

obtained in [14], but our values of q_{1S} are somewhat lower than in that work (see Fig. 16).

Figure 15 represents the fit results for the low-temperature ($T \leq 300$ K) data for $\lambda_{dt\mu-d}(\varphi)$ (a) and $\lambda_{dt\mu-t}(T)$ (b). The area limited by the straight lines corresponds to permissible values found from the fit with taking the uncertainties in density and temperature into account. The obtained fit accuracy turned out to be

$$\delta(\lambda_{dt\mu-d}) = 8\text{–}9\,\%,$$

$$\delta(\lambda_{dt\mu-t}) = 20\,\%\,(T = 300\,\text{K}) - 9\,\%\,(T = 800\,\text{K}).$$

The systematic error $\delta_{syst} = 7\%$ should be taken into account in comparing our data with theory and other measurements.

7. DISCUSSION

7.1. Muon sticking probability

As can be seen from Table 4, the experimental values of ω_s obtained by different experimental groups are in satisfactory agreement with each other. The value obtained by the direct method remarkably coincides with the one determined from the analysis of the muon losses as a function of the tritium concentration. At

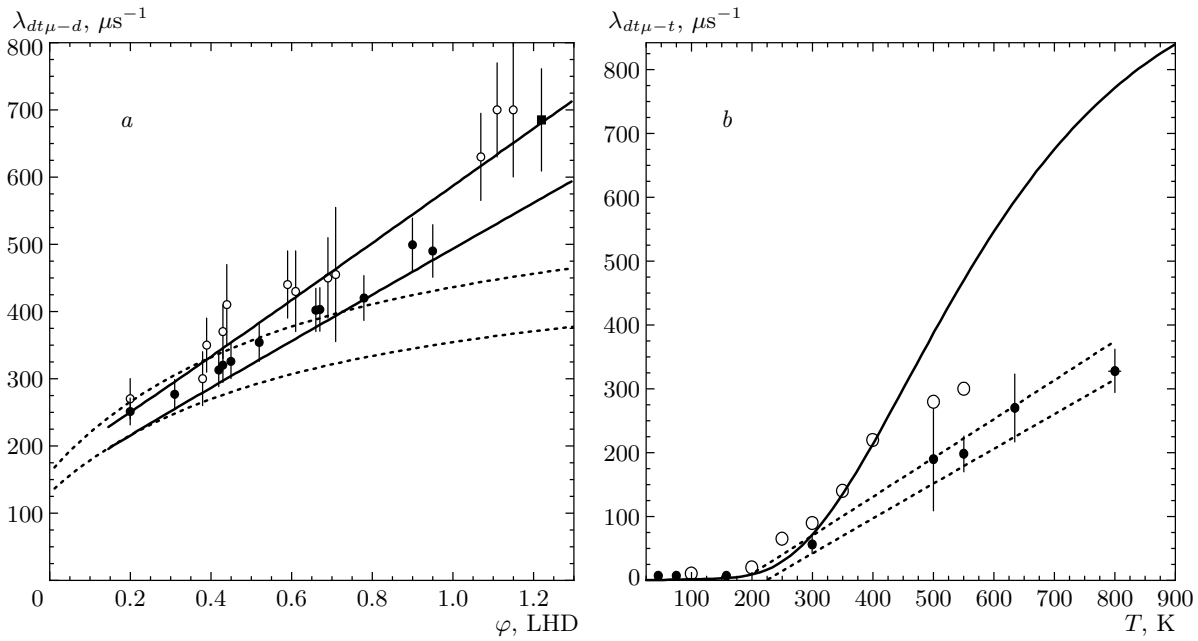

Fig. 15. a — $\lambda_{dt\mu-d}$ as a function of density for $T \leq 300$ K. Filled circles are our points for gas, empty circles are the results of LAMPF [17], the square is the result of the present paper for liquid (21). Solid lines are the permissible values found from the fit. Dashed lines are limits for the $\lambda_{dt\mu-d}$ region obtained in [14]. b — $\lambda_{dt\mu-t}$ as a function of temperature. Filled circles are our points, empty circles are the results of LAMPF [17]. The solid line is the theory result [13] for $\lambda^0_{dt\mu-t}$. Dashed lines are limits of parameterization (25)

Table 4. Comparison of the results on the ω_s obtained in different experimental and theoretical investigations

ω_s, %	Ref.	Comment
0.58	[74]	theory for $\varphi = 1.2$ LHD
0.58	[75]	theory for $\varphi = 1.2$ LHD
0.65	[76]	theory for $\varphi = 1.2$ LHD
$0.43 \pm 0.05 \pm 0.06$	[77]	LAMPF experiment for $\varphi = 1.2$ LHD
$0.48 \pm 0.02 \pm 0.04$	[78]	PSI experiment for $\varphi = 1.2$ LHD
0.532 ± 0.030	[79]	RIKEN experiment for $\varphi = 1.2$ LHD
0.505 ± 0.029	[10]	PSI experiment for $\varphi = 1.45$ LHD
$0.573 \pm 0.021^{stat} \pm 0.032^{syst}$		this experiment for $\varphi = 1.22$ LHD

the same time, some disagreement between experiment and theory remains.

7.2. q_{1S} and $\lambda_{dt\mu}$

Analysis of the experimental data confirms the theoretical conclusion about the significant role of the muon transfer from the excited $d\mu$-atom states. According to the theory, the intensity of this process turns out to depend on the tritium concentration. The probability q_{1S} of muon reaching the $d\mu$-atomic $1S$ state is successfully described by rather simple expression (20) with the same parameter a for different C_t. At the same time, contrary to the theoretical predictions, q_{1S} does not show a noticeable density dependence. These conclusions coincide with those made in the PSI paper [14].

Table 5. Results of the fit of the data for gaseous D/T at low temperatures (45–300 K) (a is the parameter of formula (20) for the q_{1S} approximation)

Parameter	Value	Conditions	
a	7.1 ± 2.5 free	T, K	φ, LHD
$\lambda_{dt\mu-d}$, μs^{-1}	326 ± 27 free	45	0.45
	403 ± 32 free	45	0.67
	490 ± 36 free	45	0.95
	320 ± 26 free	158	0.43
	402 ± 32 free	158	0.66
	499 ± 37 free	158	0.90
	292 ± 29 free	300	0.31
	313 ± 30 free	300	0.42
	380 ± 33 free	300	0.52
$\lambda_{dt\mu-t}$, μs^{-1}	7 ± 4 free	45–160	0.4–1.0
	52 ± 14 free	300	0.3–0.5

Table 6. Results of the fit of the data for gaseous D/T at high temperatures (300–800 K)

Parameter	Value	Conditions	
a	8.5 ± 2.8 free	T, K	φ, LHD
$\lambda_{dt\mu-t}$, μs^{-1}	56 ± 14 free	300	0.2–0.8
	190 ± 81 free	500	0.2–0.8
	198 ± 28 free	550	0.2–0.8
	270 ± 53 free	635	0.2–0.8
	328 ± 34 free	800	0.2–0.8
$\lambda_{dt\mu-d}$, μs^{-1}	251 ± 36 free	300	0.20
	277 ± 30 free	300	0.31
	293 ± 31 free	300	0.42
	354 ± 34 free	300	0.52
	420 ± 44 free	300	0.78
	319 ± 45 free	500–800	0.19–0.60

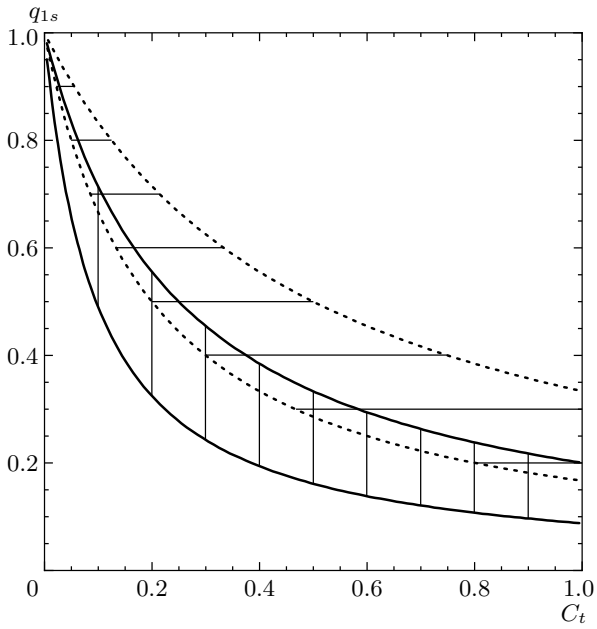

Fig. 16. q_{1S} as a function of the tritium concentration. The vertical shading is the parameterization obtained by the current fit. The horizontal shading is the PSI result [14] based on the measurements at low temperature ≤ 40 K

Table 7. Results of the common fit of the all data for gaseous D/T

Parameter	Fit result	
q_{1S}: b	7.2 ± 2.9	free
c	0 ± 1	free
λ_{dt}, μs^{-1}	280 [18, 21, 35, 36]	fixed
λ_{1-0}, μs^{-1}	1200 [68, 69]	fixed
$\lambda_{dt\mu-d}$: A_d ($T \leq 300$ K), μs^{-1}	156 ± 14	free
B_d ($T \leq 300$ K), LHD^{-1}	384 ± 21	free
C_d ($T > 300$ K), μs^{-1}	331 ± 32	free
$\lambda_{dt\mu-t}$ ($T \leq 200$ K), μs^{-1}	6 ± 6	free
A_t ($T \geq 200$ K), μs^{-1}	-117 ± 9	free
B_t ($T \geq 200$ K), K^{-1}	0.577 ± 0.028	free

As follows from the theory, at low temperatures ($T < 300$ K), the process of the $dt\mu$ formation on D_2 molecules dominates. A nontrivial density dependence $\lambda_{dt\mu-d}(\varphi)$ evidences in favor of the triple collision mechanism (7). Unfortunately, there is still no qualitative agreement between experiment and theory on the intensity of this process. It seems that the absence of a noticeable dependence of $\lambda_{dt\mu-d}$ on temperature is difficult to reconcile with the mechanism of $dt\mu$ formation on the «negative» resonance.

The experimental data on the dependence $\lambda_{dt\mu-d}(\varphi)$ obtained by different experimental groups are in satisfactory agreement. We note that the parameterization of this dependence suggested by the PSI group is not appropriate for the entire data set.

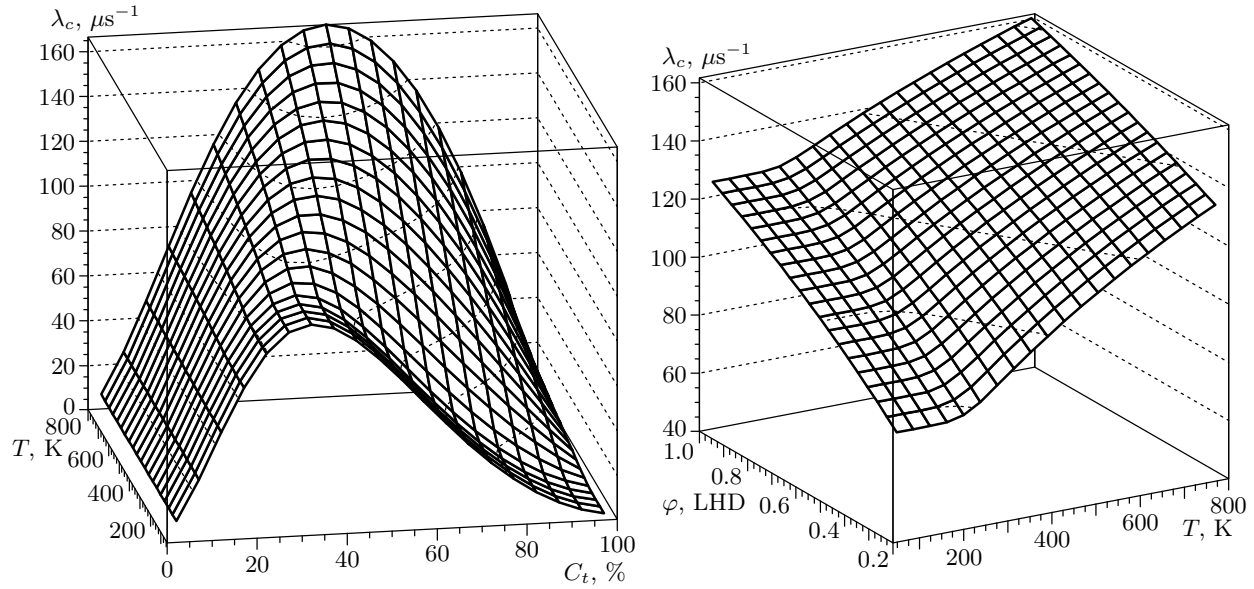

Fig. 17. Normalized cycling rate dependences on the D/T mixture conditions plotted with the use of optimum parameterizations obtained from the fit. *a* — Normalized cycling rate as a function of tritium concentration and temperature for $\varphi = 0.4$ LHD. *b* — Normalized cycling rate as a function of temperature and density for $C_t = 0.35$. The temperature region 160–300 K is smoothed

According to the theoretical predictions about the resonance positions, the process of the $dt\mu$-molecule formation on DT molecules manifests itself at high temperatures $T \approx 300$ K and rises with temperature. However, both the present results and the LAMPF data on $\lambda_{dt\mu-t}(T)$ turned out to be significantly lower than the calculated ones. This means that the intensity of the appropriate resonances is overestimated by the theory. The same conclusion follows from the analysis of the epithermal effects in the $dt\mu$ formation made by the PSI group [80]. At the same time, the TRIUMF group, making the TOF measurements of the MCF $d + t$ reaction yield as a function of the $t\mu$-atom energy [81], concluded that their data are in a satisfactory agreement with the theory. One should note, however, that the analysis in [81] is very complicated and can involve some systematic uncertainties. To clarify the situation, it is very important to make steady-state measurements at the highest temperatures $T = 1000$–2000 K, where the Maxwell distribution of the $t\mu$-atom energy overlaps the most intensive resonances.

7.3. Possible influence of epithermal effects

The parameters obtained are related to the steady-state regime, when the $t\mu$-atoms formed with the initial energy $E \geq 1$ eV have already passed through the resonances and are thermalized. However, each time after muon regeneration in the fusion reaction, the μ-atoms go through the deceleration stage, again feeling the effect of the resonances. Obviously, this leads to an increase in the cycling rate compared to values related to the Maxwell-distributed μ-atoms. This is similar to the well-studied μ-catalysis in low-temperature deuterium related to the two $d\mu$-atom spin states [82]. As in that case, there are «upper» and «lower» states with sharply different cycling rates and quick degradation of the «upper» state. By analogy, one can express the steady-state cycling rate λ_c^{ss} as

$$\lambda_c^{ss} = \lambda_c(1 + \delta),$$

where λ_c is the «bare» value.

A relative increase in the cycling rate δ can be estimated as

$$\delta \approx \alpha_{ep}\lambda_{dt\mu}^{res}/\lambda_d, \tag{26}$$

where α_{ep} is the fraction of the $t\mu$-atoms passing through the resonances during thermalization, $\lambda_{dt\mu}^{res}$ is the effective $dt\mu$-molecule formation rate in the resonance region, and λ_d is the rate with which $t\mu$-atoms leave the resonance (thermalization and back decay after the $dt\mu$ formation).

Estimations made from the calculated values of $\lambda_{dt\mu}(E_{t\mu})$ [13] and the scattering cross sections $\sigma_{t\mu+d,\,t\mu+t}$ [83] evidence that the corrections to the

steady state can be as large as tenths of percent. One can expect that the correction δ should be the smallest for the low tritium concentration because the deceleration rate in $t\mu + d$ collisions is significantly larger than in $t\mu + t$ collisions dominating at high C_t.

As a consequence, there arises a problem of correctly extracting the $dt\mu$-molecule formation rate from the dependence $\lambda_c(C_t)$ given by formula (10). The obvious conclusion is overestimation of $\lambda_{dt\mu}$ as compared with the thermalized $t\mu$-atom situation. In addition, systematic errors in the parameters of (10) can occur. Fortunately, as is seen from Figs. 13 and 14, there is satisfactory agreement between the experimental values of λ_c and expression (10). Thus, it is believed that the corresponding distortions are not so large. According to our estimations, the appropriate corrections to $\lambda_{dt\mu}$ in the region $C_t = 20$–$70\,\%$ are $\delta \approx 10$–$20\,\%$.

8. CONCLUSION

The systematic experimental investigations of the MCF process in the D/T mixture have been conducted at the JINR phasotron by the novel method. Measurements were made in a wide range of the mixture parameters — density, temperature, and tritium concentration. The variety of the experimental conditions can be seen in Fig. 17, showing the cycling rate vs mixture conditions.

Analysis of the data allows us to determine the basic MCF parameters. In general, they are in agreement with the ones obtained by other groups in the region where the experimental conditions were similar. The comparison of the experimental data with the theory confirms the efficiency of the main mechanisms considered in the MCF theory, but the full qualitative description of the process is not achieved yet.

In our opinion, it will be very important to make measurements with a D/T mixture at the highest temperatures T = 1000–2000 K, where the main resonances manifest themselves most effectively.

The authors are grateful to Prof. L. I. Ponomarev for the stimulating discussions and to D. V. Balin, G. G. Semenchuk, Yu. A. Smirenin, and N. I. Voropaev (PNPI, Gatchina), who took part in our first measurements. The work was supported by the ISTC (project № 025-95), the RF Ministry of Atomic Energy (contract № 6.25.19.19.99.969), the RF Ministry of Science and Technology (State contract № 103-7(00)-II), and the RFBR (projects №№ 97-02-16882, 98-02-16351, 00-02-17192, 03-02-16876).

The authors dedicate this article to the memory of Prof. V. P. Dzhelepov, their co-author and supervisor. Prof. V.P. Dzhelepov was the initiator of the long-term experimental research on Muon Catalyzed Fusion and till his last days was at the head of this scientific branch at JINR.

REFERENCES

1. L. I. Ponomarev, Contemp. Phys. **31**, 219 (1990).
2. W. H. Breunlich, P. Kammel, J. S. Cohen, and M. Leon, Ann. Rev. Nucl. Part. Sci. **39**, 311 (1989).
3. S. S. Gerstein, Yu. V. Petrov, and L. I. Ponomarev, Uspechi Fiz. Nauk **160**, 3 (1990).
4. L. I Ponomarev, Hyp. Interact. **138**, 15 (2001).
5. L. I. Ponomarev, in *Proc. of the Int. Workshop on Exotic Atoms*, Vienna, Austria (2002); Austrian Academy of Science Press, Vienna (2002).
6. V. V. Filchenkov and N. N. Grafov, JINR Communication E15-2003-96, Dubna (2003).
7. L. N. Bogdanova and V. V. Filchenkov, Hyp. Interact. **138**, 321 (2001).
8. C. Petitjean et al., Fusion Technology **25**, 437 (1994); Yu. V. Petrov and E. G. Sakhnovsky, Hyp. Interact. **101/102**, 647 (1996); V. Anisimov et al., Fusion Technology **39**, 198 (2001).
9. Yu. V. Petrov, Nature, London **285**, 466 (1980).
10. C. Petitjean, Hyp. Interact. **138**, 191 (2001).
11. N. I. Voropaev et al., Hyp. Interact. **138**, 331 (2001).
12. M. P. Faifman, L. I. Menshikov, and T. A. Strizh, Muon Cat. Fusion **4**, 1 (1989).
13. M. P. Faifman et al., Hyp. Interact. **101/102**, 179 (1996).
14. P. Ackerbauer et.al., Nucl. Phys. A **652**, 311 (1999).
15. P. Ackerbauer et al., Hyp. Interact. **82**, 357 (1993).
16. N. Kawamura et al., Hyp. Interact. **138**, 235 (2001).
17. S. E. Jones et al., Phys. Rev. Lett. **51**, 1757 (1983); S. E. Jones et al., Phys. Rev. Lett. **56**, 588 (1986).
18. S. E. Jones et al., Muon Cat. Fusion **1**, 21 (1987); A. J. Caffrey et al., Muon Cat. Fusion **1**, 53 (1987).
19. V. P. Dzhelepov et al., Zh. Exp. Teor. Fiz. **50**, 1235 (1966).

20. V. M. Bystritsky et al., Zh. Exp. Teor. Fiz. **76**, 460 (1979).

21. V. M. Bystritsky et al., Phys. Lett. B **94**, 476 (1980); Zh. Exp. Teor. Fiz. **80**, 1700 (1981); Pis'ma Zh. Eksp. Teor. Fiz. **53**, 877 (1981).

22. S. I. Vinitsky et al., Zh. Exp. Teor. Fiz. **74**, 849 (1978).

23. Yu. P. Averin et al., Hyp. Interact. **118**, 111 (1999).

24. V. R. Bom et al., Hyp. Interact. **118**, 103 (1999).

25. Yu. P. Averin et al., Hyp. Interact. **118**, 121 (1999).

26. V. R. Bom et al., Hyp. Interact. **138**, 213 (2001); D. L. Demin et al., JINR Communication E15-2000-157, Dubna (2000).

27. L. I. Menshikov and L. I. Ponomarev, Pis'ma Zh. Exp. Teor. Fiz. **39**, 542 (1984).

28. L. I. Menshikov and L. I. Ponomarev, Pis'ma Zh. Exp. Teor. Fiz. **42**, 12 (1985).

29. L. I. Menshikov and L. I. Ponomarev, Z. Phys. D **2**, 1 (1986).

30. V. E. Markushin, Phys. Rev. A **50**, 1137 (1994).

31. W. Czaplinski et al., Phys. Rev. A **50**, 525 (1994); Phys. Rev. A **50**, 518 (1994).

32. M. P. Faifman and L. I. Menshikov, Hyperfine Inter. **138**, 61 (2001).

33. V. E. Markushin and T. S. Jensen, Hyperfine Inter. **138**, 71 (2001).

34. A. V. Kravtsov et al., Hyperfine Inter. **138**, 103 (2001).

35. W. H. Breunlich et al., Phys. Rev. Lett. **58**, 329 (1987).

36. D. V. Balin et al., Zh. Eksp. Teor. Fiz. **92**, 1543 (1987).

37. E. Vesman, Pis'ma Zh. Eksp. Teor. Fiz. **5**, 113 (1967).

38. L. N. Bogdanova et al., Zh. Exp. Teor. Fiz. **83**, 1615 (1982).

39. L. I. Menshikov and L. I. Ponomarev, Phys. Lett. B **167**, 141 (1986).

40. M. Leon, Muon Cat. Fusion **1**, 163 (1987); Phys. Rev. A **49**, 4438 (1994).

41. Yu. V. Petrov, V. Yu. Petrov, and H. H. Schmidt, Phys. Lett. B **331**, 266 (1994).

42. A. V. Demianov et.al., JINR Communication P9-93-374, Dubna (1993).

43. D. L. Demin et al., Hyp. Interact. **119**, 349 (1999); Prib. Tekhn. Exp. **1**, 21 (1999); Preprint JINR P13-97-243, Dubna (1997).

44. V. V. Perevozchikov et al., Hyp. Interact. **119**, 353 (1999); Prib. Tekhn. Exp. **1**, 28 (1999); Preprint JINR D15-98-107, Dubna (1998).

45. V. V. Perevozchikov et al., in *Abstracts of Presentations at the Second International Workshop Interaction of Hydrogen Isotopes with Structural Materials*, IHISM-04, Sarov (2004), p. 165; to be published in Fusion Science and Technology.

46. A. A. Yukhimchuk et al., Hyp. Interact. **119**, 341 (1999).

47. A. D. Konin, JINR Communication P13-82-634, Dubna (1982).

48. V. P. Dzhelepov et al., Nucl. Instr. Meth. A **269**, 634 (1988); V. V. Filchenkov, A. D. Konin, and V. G. Zinov, Nucl. Instr. Meth. A **245**, 490 (1986); V. A. Baranov et al., Nucl. Instr. Meth. A **374**, 335 (1996); V. G. Zinov et al., JINR Communication P13-91-182, Dubna (1991).

49. V. V. Filchenkov, A. D. Konin, and A. I. Rudenko, Nucl. Instr. Meth. A **294**, 504 (1990).

50. V. G. Zinov et al., Prib. Techn. Exp. **3**, 38 (1998).

51. M. P. Malkov et al., *Guide to Physico-Technical Base of Cryogenics*, Energoatomizdat, Moscow (1973).

52. R. Prydz, K. D. Timmerhaus, and R. B. Stewart, Adv. in Cryogenic Engineering **13**, 384 (1967).

53. A. A. Yukhimchuk et al., Preprint VNIIEF 83-2002, Sarov (2002).

54. D. L. Demin et al., J. Low Temp. Phys. **120**, 45 (2000); Preprint JINR P8-99-179, Dubna (1999).

55. D. L. Demin and N. N. Grafov, *Determination of Concentrations and Nuclear Density of Hydrogen Isotope Mixtures in MCF Experiments with Liquid Tritium Target*, inner report of LNP JINR (1997).

56. L. Schellenberg, Muon Cat. Fusion **5/6**, 73 (1990/91); Hyp. Interact. **82**, 513 (1993).

57. B. Gartner et al., Hyp. Interact. **119**, 103 (1999).

58. N. Kawamura et al., Hyp. Interact. **118**, 213 (1999); N. Kawamura et al., Phys. Lett. B **465**, 74 (1999).

59. V. V. Filchenkov, A. E. Drebushko, and A. I. Rudenko, Nucl. Instr. Meth. A **395**, 237 (1997).

60. V. G. Zinov, Muon Cat. Fusion **7**, 419 (1992).

61. V. V. Filchenkov, Muon Cat. Fusion **7**, 409 (1992).

62. V. V. Filchenkov and S. M. Sadetsky, Nucl. Instr. Meth. A **480**, 771 (2002); Preprint JINR E15-2000-223, Dubna (2000).

63. V. V. Filchenkov et al., Preprint JINR E15-2002-285, Dubna (2002); Hyp. Interact. **155**, 39 (2004).

64. V. R. Bom and V. V. Filchenkov, Hyp. Interact. **119**, 365 (1999); Preprint JINR E15-98-338, Dubna (1998); V. V. Filchenkov and L. Marczis, JINR Comunication E13-88-566, Dubna (1988).

65. V. V. Filchenkov, JINR Communication E15-2000-224, Dubna (2000).

66. T. S. Jensen and V. E. Markushin, Eur. Phys. J. D **21**, 271 (2002).

67. V. V. Filchenkov and N. N. Grafov, Hyp. Interact. **138**, 241 (2001).

68. L. Bracci et.al., Phys. Lett. A **134**, 435 (1989); Muon Cat. Fusion **4**, 247 (1989).

69. D. I. Abramov, V. V. Gusev, and L. I. Ponomarev, Hyp. Interact. **138**, 275 (2001).

70. W. H. Breunlich et al., Phys. Rev. Lett. **53**, 1137 (1984); W. H. Breunlich et al., Muon Cat. Fusion **1**, 29 (1987); Ibid 67; Ibid 121.

71. T. Matsuzaki et al., Hyp. Interact. **118**, 229 (1999); Phys. Lett. B **557**, 176 (2003).

72. L. N. Bogdanova, Muon Cat. Fusion **3**, 359 (1988).

73. K. Ishida et.al., Phys. Rev. Lett. **90**, 043401 (2003); K. Ishida et al., Hyp. Intercat. **118**, 203 (1999).

74. M. Struensee and J. S. Cohen, Phys. Rev. A **38**, 44 (1988).

75. V. E. Markushin, Muon Cat. Fusion **3**, 395 (1988).

76. M. Kamimura et al., Hyp. Interact. **118**, 217 (1999).

77. S. E. Jones, S. F. Taylor, and A. N. Anderson, Hyp. Interact. **82**, 303 (1993).

78. C. Petitjean, Hyp. Interact. **82**, 273 (1993).

79. K. Ishida et al., Hyp. Interact. **138**, 225 (2001).

80. M. Jeitler et al., Phys. Rev. A **51**, 2881 (1995).

81. M. C. Fujiwara et al., Phys. Rev. Lett. **85**, 1642 (2000).

82. V. V. Filchenkov, Hyp. Interact. **101/102**, 37 (1996).

83. A. Adamczak et al., Atomic Data and Nuclear Data Tables **62**, 255 (1996); Preprint JINR E4-95-488, Dubna (1995).